

Anatomy of Vector-Like Bottom-Quark Models in the Alignment Limit of the 2-Higgs Doublet Model Type-II

A. ARHRIB^{1*}, R. BENBRIK^{2†}, M. BOUKIDI^{2‡}, S. MORETTI^{3,4§}

¹*Abdelmalek Essaadi University, Faculty of Sciences and Techniques, Tangier, Morocco*

²*Polydisciplinary Faculty, Laboratory of Fundamental and Applied Physics, Cadi Ayyad University, Sidi Bouzid, B.P. 4162, Safi, Morocco*

³*Department of Physics & Astronomy, Uppsala University, Box 516, SE-751 20 Uppsala, Sweden*

⁴*School of Physics & Astronomy, University of Southampton, Southampton, SO17 1BJ, United Kingdom*

Abstract

Expanding upon our ongoing investigation of Vector-Like Quark (VLQ) phenomenology within a 2-Higgs Doublet Model (2HDM) framework, in this paper, we complement a previous one dedicated to Vector-Like Top-quarks (VLTs) by studying Vector-Like Bottom-quarks (VLBs), specifically focusing on their behavior in the alignment limit of a Type-II Yukawa structure. We examine the potential for detecting VLBs at the Large Hadron Collider (LHC) and analyze their decay signatures, encompassing both Standard Model (SM) processes and exotic decays. The objective is to differentiate among singlet, doublet, and triplet configurations of VLBs by identifying distinct decay patterns, thereby providing insights into the structure of Beyond the SM (BSM) physics.

*aarhrib@gmail.com

†r.benbrik@uca.ac.ma

‡mohammed.boukidi@ced.uca.ma

§stefano.moretti@physics.uu.se; s.moretti@soton.ac.uk

1 Introduction

Building on the pivotal discovery of the Higgs boson during the LHC Run 1 at CERN and the subsequent detailed analyses of its properties by the ATLAS and CMS collaborations [1, 2], herein, we delve deeper into the exploration of Vector-Like Quarks (VLQs), particularly focusing on the Bottom-type VLQs (VLBs), in this continuation of our previous research [3]. The identification of the Higgs boson has largely validated the Standard Model (SM) predictions, yet certain anomalies observed across various production and decay channels signal the potential for Beyond the Standard Model (BSM) physics, inviting further investigation into the role of VLBs.

In the backdrop of the 2-Higgs Doublet Model (2HDM) [4, 5], which introduces additional Higgs bosons (H , A , and H^\pm) in addition to the discovered SM-like one (h), our study is aimed at uncovering the implications of including VLBs with unique Electro-Weak (EW) quantum numbers and non-Yukawa type couplings. This research not only seeks to address the anomalies noted in Higgs boson measurements but also to extend the analysis conducted on Top-type VLQs (VLTs) [3], by examining the exotic decay channels of VLBs into these new Higgs states, a subject that remains underexplored at the LHC.

Our motivation is driven by the potential of VLBs to decay into 2HDM additional Higgs bosons, which could evade detection by current LHC search strategies, which are focused on SM decay modes, and to assess the model alignment with EW Precision Observables (EWPOs). Through this work, we aim at contributing to a deeper understanding of VLBs within the BSM framework, emphasizing the significance of their exotic decay channels in revealing new aspects of particle physics.

This paper, advancing our series on VLQs within a 2HDM context [6–27], is structured to firstly elaborate on the theoretical foundations of the 2HDM and VLBs, followed by a detailed exploration of the decay patterns of VLBs and their potential implications for LHC detection and characterization. By leveraging insights from our previous work on VLTs, specifically on the 2HDM Type-II [3], we endeavor to provide a comprehensive perspective on the capabilities of VLBs to illuminate new physics phenomena.

The paper is structured as follows. In the next section, we discuss our model. In the following section we present and discuss our results. Then we summarize and draw our conclusions.

2 Model description

2.1 Formalism

In this paper, we extend the work presented in Ref. [3], which established a CP-conserving 2HDM Type-II also featuring VLQ representations, wherein the phenomenology of this BSM setup was accessed via VLT decay dynamics, while here we will establish the one of the VLB sector.

The 2HDM part of our scenario produces the canonical set of Higgs bosons: two CP-even states, with h being the lightest and H the heaviest, a CP-odd state, A , and a pair of charged Higgs bosons, H^\pm . As tree-level Flavor Changing Neutral Currents (FCNCs) are very

constrained by experiment, we impose a \mathbb{Z}_2 symmetry, such that $\Phi_1 \rightarrow \Phi_1$ and $\Phi_2 \rightarrow -\Phi_2$, on the Higgs fields. The resulting Higgs potential (softly broken by dimension-2 terms $\propto m_{12}^2$) can be written as

$$\begin{aligned} \mathcal{V} = & m_{11}^2 \Phi_1^\dagger \Phi_1 + m_{22}^2 \Phi_2^\dagger \Phi_2 - \left(m_{12}^2 \Phi_1^\dagger \Phi_2 + \text{H.c.} \right) + \frac{1}{2} \lambda_1 \left(\Phi_1^\dagger \Phi_1 \right)^2 + \frac{1}{2} \lambda_2 \left(\Phi_2^\dagger \Phi_2 \right)^2 \\ & + \lambda_3 \Phi_1^\dagger \Phi_1 \Phi_2^\dagger \Phi_2 + \lambda_4 \Phi_1^\dagger \Phi_2 \Phi_2^\dagger \Phi_1 + \left[\frac{1}{2} \lambda_5 \left(\Phi_1^\dagger \Phi_2 \right)^2 + \text{H.c.} \right]. \end{aligned} \quad (1)$$

By choosing real Vacuum Expectation Values (VEVs) for the two Higgs doublet fields, v_1 and v_2 , and demanding m_{12}^2 and λ_5 to be real, the potential is CP-conserving. The free independent parameters are here taken to be the four masses, m_h , m_H , m_A and m_{H^\pm} , the soft \mathbb{Z}_2 -breaking parameter m_{12} , the VEV ratio $\tan \beta = v_2/v_1$ and the mixing term $\sin(\beta - \alpha)$, where the angle α diagonalizes the CP-even mass matrix. When we impose that no (significant) tree-level FCNCs are present in the theory using the (softly broken) \mathbb{Z}_2 symmetry, we end up with four different Yukawa versions of the model. These are: Type-I, where only Φ_2 couples to all fermions; Type-II, where Φ_2 couples to up-type quarks and Φ_1 couples to charged leptons and down-type quarks; Type-Y (or Flipped), where Φ_2 couples to charged leptons and up-type quarks and Φ_1 couples to down-type quarks; Type-X (or Lepton Specific), where Φ_2 couples to quarks and Φ_1 couples to charged leptons¹.

The gauge invariant structures that have multiplets with definite $SU(3)_C \times SU(2)_L \times U(1)_Y$ quantum numbers appear in the interactions of new VLQs with the SM states via renormalizable couplings. The set of VLQ representations is indicated by:

$$\begin{aligned} B_{L,R}^0 & & (\text{singlets}), \\ (B^0 Y)_{L,R}, \quad (T^0 B^0)_{L,R} & & (\text{doublets}), \\ (X T^0 B^0)_{L,R}, \quad (T^0 B^0 Y)_{L,R} & & (\text{triplets}). \end{aligned} \quad (2)$$

We use in this section a zero superscript to distinguish the weak from the mass eigenstates. The Electro-Magnetic (EM) charges of the new VLQs are $Q_T = 2/3$, $Q_B = -1/3$, $Q_X = 5/3$ and $Q_Y = -4/3$. Note that T and B carry the same EM charge as the SM top and bottom quarks, respectively.

The physical up-type quark mass eigenstates may, in general, contain non-zero $Q_{L,R}^0$ (with Q being the VLQ field) components, when new fields $T_{L,R}^0$ of charge $2/3$ and non-standard isospin assignments are added to the SM. This situation leads to a deviation in their couplings to the Z boson. Atomic parity violation experiments and the measurement of R_c at LEP give some constraints on these deviations for the up and charm quarks which are far stronger than for the top quark. In the Higgs basis, the Yukawa Lagrangian contains the following terms:

$$-\mathcal{L} \supset y^u \bar{Q}_L^0 \tilde{H}_2 u_R^0 + y^d \bar{Q}_L^0 H_1 d_R^0 + M_u^0 \bar{u}_L^0 u_R^0 + M_d^0 \bar{d}_L^0 d_R^0 + \text{H.c.} \quad (3)$$

Here, u_R runs over (u_R, c_R, t_R, T_R) while d_R runs over (d_R, s_R, b_R, B_R) .

We now turn to the mixing of the new partners to the third generation, y_u and y_d , which are 3×4 Yukawa matrices. In fact, in the light of the above constraints, it is very reasonable to assume that only the top quark t ‘‘mixes’’ with T . In this case, the 2×2 unitary matrices $U_{L,R}^u$ define the relation between the charge $2/3$ weak and mass eigenstates:

$$\begin{pmatrix} t_{L,R} \\ T_{L,R} \end{pmatrix} = U_{L,R}^u \begin{pmatrix} t_{L,R}^0 \\ T_{L,R}^0 \end{pmatrix} = \begin{pmatrix} \cos \theta_{L,R}^u & -\sin \theta_{L,R}^u e^{i\phi_u} \\ \sin \theta_{L,R}^u e^{-i\phi_u} & \cos \theta_{L,R}^u \end{pmatrix} \begin{pmatrix} t_{L,R}^0 \\ T_{L,R}^0 \end{pmatrix}. \quad (4)$$

¹In this paper, we will be discussing only Type-II.

In contrast to the up-type quark sector, the addition of new fields $B_{L,R}^0$ of charge $-1/3$ in the down-type quark sector results in four mass eigenstates, d, s, b, B . Measurements of R_b at LEP set tight constraints on the b mixing with the new fields that are stronger than for mixing with the lighter quarks d, s . In this case, then, 2×2 unitary matrices $U_{L,R}^d$ define the dominant $b - B$ mixing as

$$\begin{pmatrix} b_{L,R} \\ B_{L,R} \end{pmatrix} = U_{L,R}^d \begin{pmatrix} b_{L,R}^0 \\ B_{L,R}^0 \end{pmatrix} = \begin{pmatrix} \cos \theta_{L,R}^d & -\sin \theta_{L,R}^d e^{i\phi_d} \\ \sin \theta_{L,R}^d e^{-i\phi_d} & \cos \theta_{L,R}^d \end{pmatrix} \begin{pmatrix} b_{L,R}^0 \\ B_{L,R}^0 \end{pmatrix}. \quad (5)$$

To ease the notation, we have dropped the superscripts $u(d)$ whenever the mixing occurs only in the up(down)-type quark sector. Additionally, we sometime use the shorthand notations $s_{L,R}^{u,d} \equiv \sin \theta_{L,R}^{u,d}$, $c_{L,R}^{u,d} \equiv \cos \theta_{L,R}^{u,d}$, etc. (More details on this Lagrangian formalism are shown in the Appendix.)

This Lagrangian contains all the relevant phenomenological information, as follows:

- (i) the modifications of the SM couplings that might show indirect effects of new quarks can be found in the terms that do not contain VLQ fields;
- (ii) the terms relevant for LHC phenomenology (i.e., VLQ production and decay) are those involving a heavy and a light quark;
- (iii) terms with two VLQs are relevant for their contribution to oblique corrections (i.e., to the S, T and U parameters of the EWPOs).

In the weak eigenstate basis, the diagonalization of the mass matrices makes the Lagrangian of the third generation and heavy quark mass terms such as

$$\begin{aligned} \mathcal{L}_{\text{mass}} = & - (\bar{t}_L^0 \quad \bar{T}_L^0) \begin{pmatrix} y_{33}^u \frac{v}{\sqrt{2}} & y_{34}^u \frac{v}{\sqrt{2}} \\ y_{43}^u \frac{v}{\sqrt{2}} & M^0 \end{pmatrix} \begin{pmatrix} t_R^0 \\ T_R^0 \end{pmatrix} \\ & - (\bar{b}_L^0 \quad \bar{B}_L^0) \begin{pmatrix} y_{33}^d \frac{v}{\sqrt{2}} & y_{34}^d \frac{v}{\sqrt{2}} \\ y_{43}^d \frac{v}{\sqrt{2}} & M^0 \end{pmatrix} \begin{pmatrix} b_R^0 \\ B_R^0 \end{pmatrix} + \text{H.c.}, \end{aligned} \quad (6)$$

with M^0 a bare mass term², y_{ij}^q , $q = u, d$, Yukawa couplings and $v = 246$ GeV the Higgs VEV in the SM. Using the standard techniques of diagonalization, the mixing matrices are obtained by

$$U_L^q \mathcal{M}^q (U_R^q)^\dagger = \mathcal{M}_{\text{diag}}^q, \quad (7)$$

with \mathcal{M}^q the two mass matrices in Eq. (6) and $\mathcal{M}_{\text{diag}}^q$ the diagonals ones. To check the consistency of our calculation, the corresponding 2×2 mass matrix reduces to the SM quark mass term if either the T or B quarks are absent.

Notice also that, in multiplets with both T and B quarks, the bare mass term is the same for the up- and down-type quark sectors. For singlets and triplets one has $y_{43}^q = 0$ whereas for doublets $y_{34}^q = 0$. Moreover, for the (XTB) triplet, one has $y_{34}^d = \sqrt{2}y_{34}^u$ and for the (TBY) triplet one has $y_{34}^u = \sqrt{2}y_{34}^d$ ³.

²Note that this bare mass term is not related to the Higgs mechanism: it is gauge invariant and can appear as such in the Lagrangian, or it can be generated by a Yukawa coupling to a scalar multiplet that acquires a VEV $v' \gg v$.

³We write the triplets in the spherical basis, hence, the $\sqrt{2}$ factors stem from the relation between the Cartesian and spherical coordinates of an irreducible tensor operator of rank 1 (vector).

The mixing angles in the left- and right-handed sectors are not independent parameters. From the mass matrix bi-unitary diagonalization in Eq. (7) one finds:

$$\begin{aligned}\tan 2\theta_L^q &= \frac{\sqrt{2}|y_{34}^q|vM^0}{(M^0)^2 - |y_{33}^q|^2v^2/2 - |y_{34}^q|^2v^2/2} \quad (\text{singlets, triplets}), \\ \tan 2\theta_R^q &= \frac{\sqrt{2}|y_{43}^q|vM^0}{(M^0)^2 - |y_{33}^q|^2v^2/2 - |y_{43}^q|^2v^2/2} \quad (\text{doublets}),\end{aligned}\tag{8}$$

with the relations

$$\begin{aligned}\tan \theta_R^q &= \frac{m_q}{m_Q} \tan \theta_L^q \quad (\text{singlets, triplets}), \\ \tan \theta_L^q &= \frac{m_q}{m_Q} \tan \theta_R^q \quad (\text{doublets}),\end{aligned}\tag{9}$$

with $(q, m_q, m_Q) = (u, m_t, m_T)$ and (d, m_b, m_B) , so one of the mixing angles is always dominant, especially in the down-type quark sector. In addition, for the triplets, the relations between the off-diagonal Yukawa couplings lead to relations between the mixing angles in the up- and down-type quark sectors,

$$\begin{aligned}\sin 2\theta_L^d &= \sqrt{2} \frac{m_T^2 - m_t^2}{m_B^2 - m_b^2} \sin 2\theta_L^u \quad (XTB), \\ \sin 2\theta_L^d &= \frac{1}{\sqrt{2}} \frac{m_T^2 - m_t^2}{m_B^2 - m_b^2} \sin 2\theta_L^u \quad (TBY).\end{aligned}\tag{10}$$

The masses of the heavy VLQs deviate from M^0 due to the non-zero mixing with the SM quarks plus, for doublets and triplets, the masses of the different components of the multiplet are related. Altogether, these relations show that all multiplets except the (TB) doublet can be parametrized by a mixing angle, a heavy quark mass and a CP-violating phase that enters some couplings, with the latter being ignored for the observables considered in this paper. In the case of the (TB) doublet, there are two independent mixing angles and two CP-violating phases for the up- and down-type quark sectors, with - again - the latter set to zero in our analysis. Hereafter, we refer to such a construct as the 2HDM+VLQ scenario, distinguishing between the singlet, doublet and triplet cases. In the present paper, though, given the emphasis on VLBs, as opposed to VLTs, we will treat the (B) singlet, (BY) and (TB) doublets as well as (XTB) and (TBY) triplets whereas we will not deal with the (T) singlet and (XT) doublet representations, as their study was tackled in Ref. [3]. Finally, as discussed in the abstract, we decided to work in the so-called ‘‘alignment limit’’ of the 2HDM, wherein we fix $m_h = 125$ GeV (so that the lightest neutral Higgs state of the 2HDM is the discovered one) and we have further taken $m_{12}^2 = m_A^2 \frac{\tan^2 \beta}{1 + \tan^2 \beta}$ for the soft \mathbb{Z}_2 -breaking parameter.

2.2 Implementation and validation

In this subsection, we briefly describe our implementation of the aforementioned BSM scenario. We have used 2HDMC-1.8.0 [28] as a base platform for our 2HDM+VLQ setup⁴. As a first step, the above Lagrangian components were implemented into `FeynRules-2.3` [29] to generate the proper spectrum of masses and couplings. With the help of this program, we have then

⁴A public release of it is in progress: herein, the analytical expressions for the Feynman rules of the interaction vertices of our 2HDM+VLQ model have been implemented as a new class while several new tree-level VLQ decays have explicitly been coded alongside those of Higgs bosons into VLQs themselves.

generated `FeynArts-3.11` [30, 31] and `FormCalc-9.10` [32, 33] model files as well as Universal FeynRules Output (UFO) interfaces to be used in `MadGraph-3.4.2` [34]. As consistency checks, we have verified the cancellation of Ultra-Violet (UV) divergences as well as the renormalization scale independence of all relevant loop-level processes.

2.3 EWPOs in VLQ

EWPOs can restrict severely the parameter space of BSM physics scenarios. In our 2HDM+VLQ setup (Such analytic results for the S and T parameters have been presented in [35].), for both S and T , we have two additive contributions: one from VLQs and the other from 2HDM Higgses. The latter is very well known and we have taken it from [13] while the former can be calculated using the approach of Ref. [14], as it has been done in Ref. [15]. However, the approach of Ref. [14] works only for the singlet and doublet representations of the new fermions and cannot be applied to the triplet cases. For all various VLQ representations considered here, we have computed the S and T parameters with the use of the aforementioned `FeynArts` and `FormCalc` packages using dimensional regularization. The analytic results were obtained as a combination of standard Passarino-Veltman (PV) functions. We checked both analytically and numerically that our results for S and T are UV finite and renormalization scale independent. For the T parameter, we have compared our results to Refs. [14, 15] and found good agreement in the case of singlet and doublet. In the case of the triplet representations (XTB) and (TBY), our result disagrees with Ref. [15]. Furthermore, for the S parameter, our results disagree with those of Ref. [15]. In fact, Ref. [15] simply extends the result of the singlet and doublet cases from Ref. [14] to the triplet one. The author of Ref. [36] derives the correct expression for S and T in the case of the (XTB) triplet using the approach of Ref. [14]. We recomputed from scratch the results for the (XTB) and (TBY) triplet cases, then rederived S and T in terms of PV functions and, crucially, did not neglect the external momentum of the gauge bosons. We are confident of the correctness of our findings, as they were derived in two different ways. A major source of disagreement would be the fact that Ref. [15] uses a simple approximation for the S parameter, which consists in neglecting the external momentum of the gauge bosons. We also cross-checked with a new calculation [36, 37] and found good agreement for the T parameter. However, we should mention that, for the S parameter, we use the complete analytical result and, again, did not neglect any external momentum as it is usually done [37].

2.4 Constraints

In this section, we list the constraints that we have used to check the validity of our results. From the theoretical side, we have the following requirements:

- **Unitarity** constraints require the S -wave component of the various (pseudo)scalar-(pseudo)scalar, (pseudo)scalar-gauge boson, and gauge-gauge bosons scatterings to be unitary at high energy [38].
- **Perturbativity** constraints impose the following condition on the quartic couplings of the scalar potential: $|\lambda_i| < 8\pi$ ($i = 1, \dots, 5$) [4].
- **Vacuum stability** constraints require the potential to be bounded from below and positive in any arbitrary direction in the field space, as a consequence, the λ_i parameters

should satisfy the conditions as [39, 40]:

$$\begin{aligned}\lambda_1 > 0, \quad \lambda_2 > 0, \quad \lambda_3 > -\sqrt{\lambda_1\lambda_2}, \\ \lambda_3 + \lambda_4 - |\lambda_5| > -\sqrt{\lambda_1\lambda_2}.\end{aligned}\tag{11}$$

- **Constraints from EWPOs**, implemented through the oblique parameters, S and T [41], require that, for a parameter point of our model to be allowed, the corresponding $\chi^2(S^{2\text{HDM-II}} + S^{\text{VLQ}}, T^{2\text{HDM-II}} + T^{\text{VLQ}})$ is within 95% Confidence Level (CL) in matching the global fit results [42]:

$$S = 0.05 \pm 0.08, \quad T = 0.09 \pm 0.07, \quad \rho_{S,T} = 0.92 \pm 0.11. \quad (\text{For } U = 0)$$

Note that unitarity, perturbativity, vacuum stability, as well as S and T constraints, are enforced through the public code `2HDMC-1.8.0` [28].

From the experimental side, we evaluated the following:

- **Constraints from the SM-like Higgs-boson properties** are taken into account by using `HiggsSignal-3` [43, 44] via `HiggsTools` [45]. We require that the relevant quantities (signal strengths, etc.) satisfy $\Delta\chi^2 = \chi^2 - \chi_{\min}^2$ for these measurements at 95% CL ($\Delta\chi^2 \leq 6.18$).
- **Constraints from direct searches at colliders**, i.e., LEP, Tevatron, and LHC, are taken at the 95% CL and are tested using `HiggsBounds-6` [46–49] via `HiggsTools`. Including the most recent searches for neutral and charged scalars.
- **Constraints from $b \rightarrow s\gamma$** : To align with the measurements of $b \rightarrow s\gamma$, we have set the mass of the charged Higgs boson to be greater than 600 GeV, based on our previous work [27], which showed that the inclusion of VLQ in the Type-II 2HDM allows for a relaxation of the $b \rightarrow s\gamma$ limit with larger mixing angles. However, EWPOs impose constraints on these angles to be small, leading us to navigate around the typical 580 GeV threshold in the Type-II 2HDM.

2.5 Direct search constraints

In this section, we explore the implications of experimental constraints on the properties of additional Higgs states and VLQs within our 2HDM+VLQ framework. The oblique parameters S and T play a crucial role by imposing stringent limits on the VLQ mixing angles, as elaborated in our previous work [27] and in the previous subsection. This limitation leads to small mixing angles, allowing VLQ masses to start from as low as 1000 GeV without conflicting with existing LHC exclusions. This pattern holds true across singlet, doublet and triplet VLQ configurations.

2.6 VLQs contribution to Higgs production and decay

VLQs contribute to the loop diagrams for Higgs production via gluon-gluon fusion and Higgs decay into two photons. However, in our study, their contributions are relatively small. This

Parameters	Scanned ranges
m_h	125
m_A	[300, 1000]
m_H	[300, 1000]
m_{H^\pm}	[600, 1000]
$\tan \beta$	[1, 20]
m_B	[1000, 2000]
$\sin \theta_L^{u,d}$	[-0.5, 0.5]
$\sin \theta_R^{u,d}$	[-0.5, 0.5]

Table 1: 2HDM and VLQs parameters for all scenarios with their scanned ranges. Masses are in GeV. The phases ϕ_u and ϕ_d are set to zero.

is partly because VLQs tend to decouple from the process as their masses increase and also due to the mixing angles terms ($s_{L,R}^d$) appear in the coupling hTT (refer to Table XIV in the appendix) are restricted by the EWPOs resulting in small values for these terms (The largest allowed mixing angle is approximately $s_{L,R}^d \sim 0.2$), further suppressed by their squares. However, it's noteworthy that the primary contribution arises from modifications in the htt .

For the processes $gg \rightarrow H$ (or $H \rightarrow gg$) and $H \rightarrow \gamma\gamma$, the contribution of all quarks of the same charge to the corresponding amplitudes is determined by the expression:

$$F_q = \sum_i Y_{ii} A_{1/2} \left(\frac{M_H^2}{4m_i^2} \right), \quad (12)$$

Here, the sum runs over t, T for $q = u$ and over b, B for $q = d$. The couplings to the Higgs Y_{ii} are defined in Table XIV of the appendix, and the function $A_{1/2}$ is defined in [50].

Our analysis reveals that, across all considered scenarios, the branching ratio $\mathcal{BR}(h \rightarrow gg)$ experiences a decrease of up to 10%, primarily due to modifications in the htt coupling. Similarly, the branching ratio $\mathcal{BR}(h \rightarrow \gamma\gamma)$ decreases by up to 3%, also attributed to modifications in the htt coupling. Meanwhile, the contributions of the new terms hTT are deemed negligible, as discussed earlier.

3 Results and discussions

In discussing our results, we deal with these in turn for the different VLQ representations.

3.1 2HDM with (B) singlet

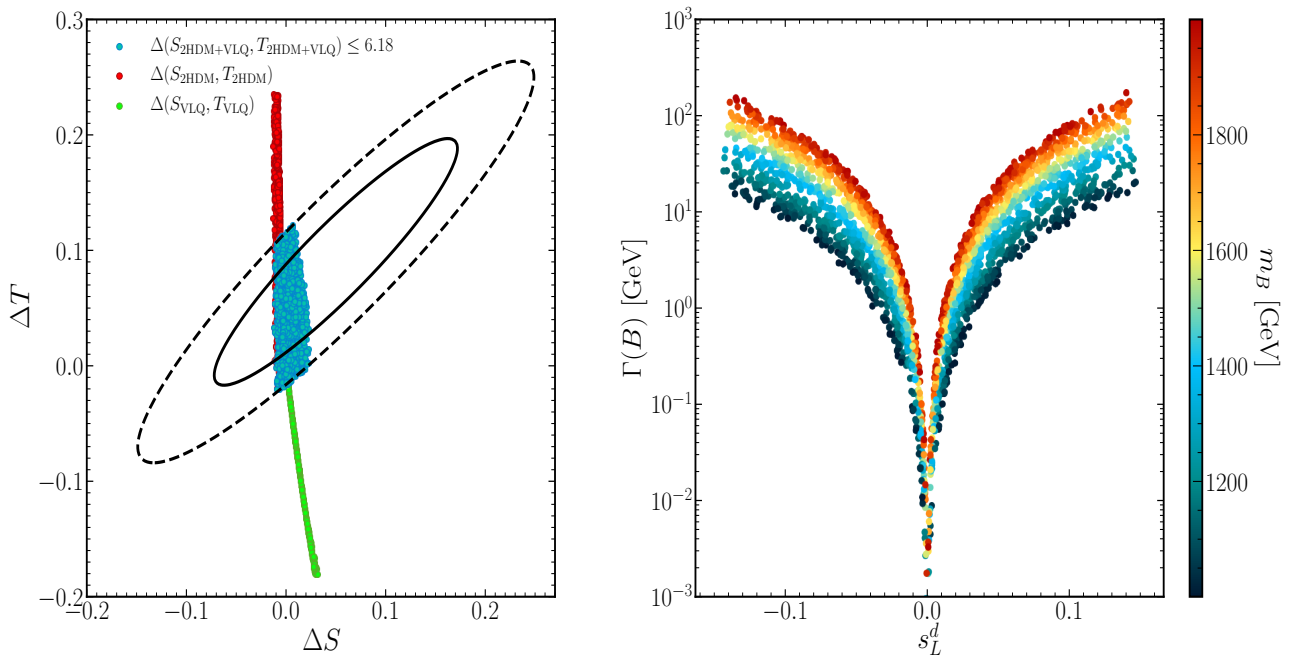


Figure 1: (Left) Scatter plots of randomly generated points superimposed onto the fit limits in the $(\Delta S, \Delta T)$ plane from EWPO data at 95% CL with a correlation of 92%. Here, we illustrate the 2HDM and VLQ contributions separately and also the total one. (Right) The B width $\Gamma(B)$ ($\equiv \Gamma_B$) as a function of $s_L^d \equiv \sin \theta_L$ with m_B indicated as a color gauge.

In Fig. 1, we conduct an analysis across the 2HDM parameters, including the Higgs boson masses, $\tan \beta$, $\sin(\beta - \alpha)$ and m_{12} , along with the mass of the singlet VLB, m_B , and the fermionic mixing angle, $\sin \theta_L$, as outlined in Tab. 1. In the left section of Fig. 1, we present our findings on how the 2HDM scalars and the sole VLQ in this 2HDM+VLQ scenario affect the S and T parameters. We detail these influences both individually and collectively. The S parameter contributions from the VLQ and 2HDM sectors, denoted as $S_{\text{VLQ}, 2\text{HDM}}$, respectively, are relatively small. In contrast, for the T parameter, the $T_{\text{VLQ}, 2\text{HDM}}$ effects can be substantial and often exhibit opposite signs. This variance allows for significant cancellations, especially since $T_{2\text{HDM}}$ can have either sign while T_{VLQ} is almost invariably negative. Specifically, a large negative value for T_{VLQ} can arise with high $\sin \theta_L$ values and a correspondingly large positive $T_{2\text{HDM}}$ term can occur in the 2HDM when there is a considerable mass splitting among the heavy Higgs bosons. It is important to note that, within this representation, the constraints imposed by the S and T parameters are more stringent than those from R_b limits [8].

The right panel of Fig. 1 displays our analysis projected onto the $(\sin \theta_L, \Gamma(B))$ plane⁵, illustrating that the mixing angle $|\sin \theta_L|$ typically does not exceed 0.15 across the entire m_B range. For minimal mixing ($|\sin \theta_L| < 0.1$), the total width is relatively small, often a few GeV or less. In contrast, for more large mixing ($|\sin \theta_L| \approx 0.1 - 0.15$) combined with large m_B values, the total width may vary between 10 and 100 GeV. These $\Gamma(B)$ values are likely to be comparable to the experimental resolution of reconstructed VLBs, suggesting that the width of the VLB could be limited to a maximum of 10% of its mass.

This detailed analysis underscores the critical impact of incorporating additional degrees of

⁵Here, $\Gamma(B)$, at times also denoted by Γ_B is the VLB total width.

freedom from both the VLQ sector and 2HDM one. Their integration enables a diverse array of solutions, accommodating lighter m_B masses (~ 1 TeV) and extensive mixing angles $|\sin \theta_L|$. This, in turn, could significantly enhance $pp \rightarrow B\bar{B}$ production rates at the LHC (see Fig. 2) as well as the likelihood of B decays into heavy (pseudo)scalar Higgs states obtained from the 2HDM sector with notable frequencies, as we shall see.

In Fig. 2, we depict the pair production cross-section⁶ $\sigma(pp \rightarrow Q\bar{Q})$ at the next-to-next-to-leading order (NNLO) using the sets CTEQ6L1 [51] parton densities, as a function of their mass m_Q . The curves are depicted in blue and orange, corresponding to centre of mass energies of 13 TeV and 14 TeV, respectively.

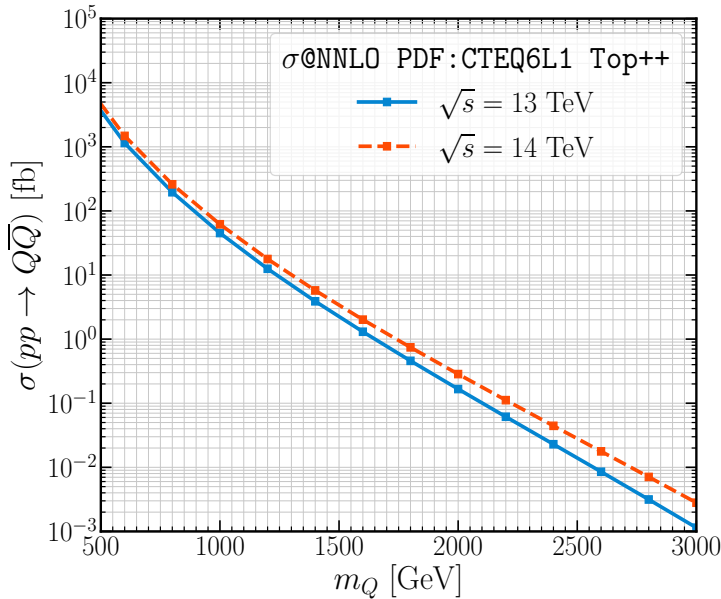


Figure 2: Pair production cross-section $\sigma(pp \rightarrow Q\bar{Q})$, computed at NNLO using Top++ [52] for center-of-mass energies $\sqrt{s} = 13$ TeV (blue) and $\sqrt{s} = 14$ TeV (orange), respectively.

Advancing our discussion to the Branching Ratios (\mathcal{BR}) associated with the B state, we find the scenario within the SM, supplemented by an additional singlet bottom, mirrors closely the dynamics outlined for the singlet VLT scenario tackled in Ref. [3]. The distribution of \mathcal{BR} s among $B \rightarrow W^-t$, $B \rightarrow Zb$ and $B \rightarrow hb$ remains approximately at 50%, 25% and 25%, respectively, as for a VLT. Remarkably, these distributions show limited sensitivity to variations in the $\sin \theta_L$ mixing angle and are bound by a sum rule that ensures their collective contribution to the B state decay processes into SM final states respects

$$\mathcal{BR}(B \rightarrow \text{SM}) = \mathcal{BR}(B \rightarrow W^-t) + \mathcal{BR}(B \rightarrow Zb) + \mathcal{BR}(B \rightarrow hb) = 1. \quad (13)$$

The introduction of additional decay pathways through (pseudo)scalar channels such as $B \rightarrow H^+t$, $B \rightarrow Ab$ and $B \rightarrow Hb$ introduces a significant shift. This evolution not only diversifies the decay mechanisms but also modifies the constraints previously established by direct B searches at the LHC, prompting an updated sum rule:

$$\begin{aligned} \mathcal{BR}(B \rightarrow \text{SM}) + \mathcal{BR}(B \rightarrow \text{non SM}) &= 1, \\ \mathcal{BR}(B \rightarrow \text{non SM}) &= \mathcal{BR}(B \rightarrow H^+t) + \mathcal{BR}(B \rightarrow Ab) + \mathcal{BR}(B \rightarrow Hb). \end{aligned} \quad (14)$$

⁶Note that the pair production of VLQs is model independent and relies solely on their mass.

In Fig. 3, we depict the correlation between the decay processes of the B state into SM particles and through novel pathways, organized as follows: $B \rightarrow hb, Hb$ (left), $B \rightarrow Zb, Ab$ (middle), and $B \rightarrow W^+b, H^+b$ (right). It is observed that when non-SM decay channels become kinematically open, the $\mathcal{BR}(B \rightarrow H^+t)$ begins to rival the $\mathcal{BR}(B \rightarrow W^+t)$ especially for low $\tan \beta \sim 1$. A similar competitive relationship is noted between $\mathcal{BR}(B \rightarrow Hb)$ and $\mathcal{BR}(B \rightarrow Ab)$ but for medium $\tan \beta$.

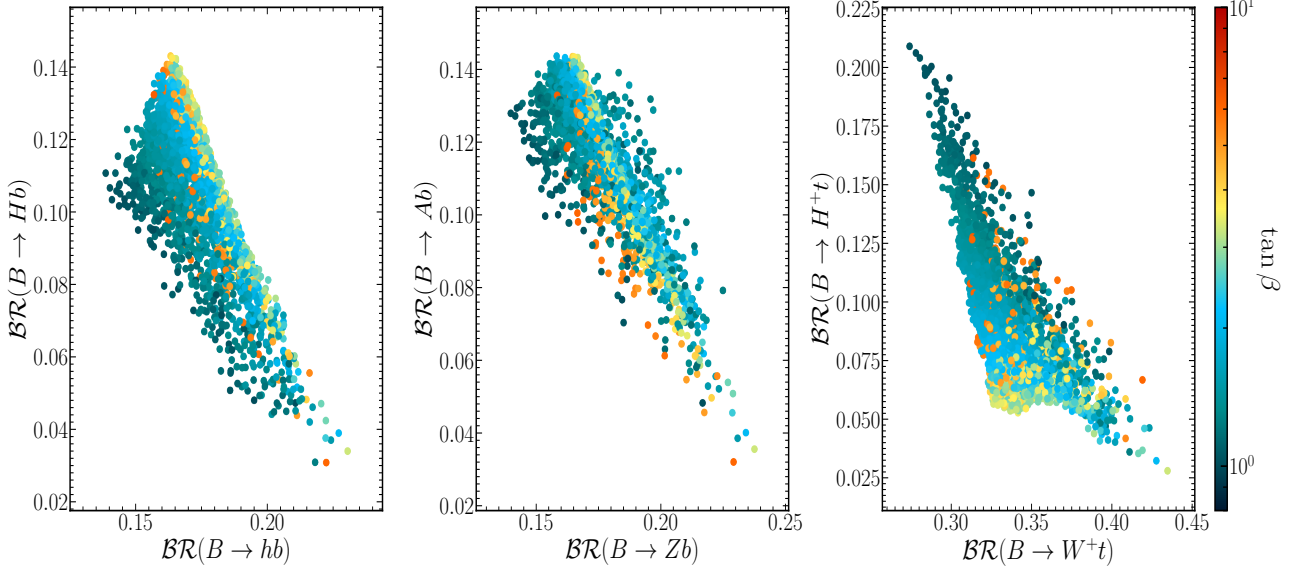


Figure 3: The correlation between $\mathcal{BR}(B \rightarrow hb)$ and $\mathcal{BR}(B \rightarrow Hb)$ (left), $\mathcal{BR}(B \rightarrow Zb)$ and $\mathcal{BR}(B \rightarrow Ab)$ (middle) as well as $\mathcal{BR}(B \rightarrow W^+t)$ and $\mathcal{BR}(B \rightarrow H^+t)$ (right) with $\tan \beta$ indicated in the color gauge.

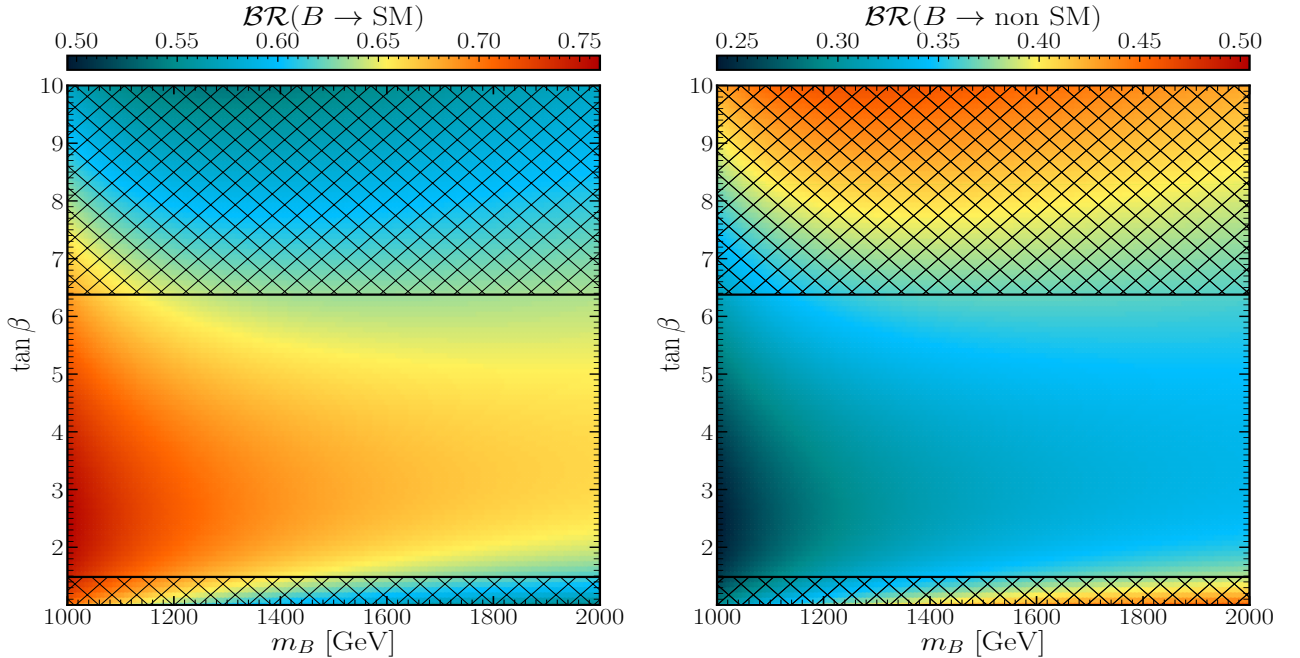


Figure 4: The $\mathcal{BR}(B \rightarrow \text{SM})$ (left) and $\mathcal{BR}(B \rightarrow \text{non SM})$ (right) mapped onto the $(m_B, \tan \beta)$ plane, with $\sin \theta_L = 0.045$, $\sin(\beta - \alpha) = 1$, $m_h = 125$ GeV, $m_H = 585$, $m_A = 582$ GeV, and $m_{H^\pm} = 650$ GeV (recall that $m_{12}^2 = m_A^2 \tan \beta / (1 + \tan^2 \beta)$). Here, the shaded areas are excluded by HiggsBounds ($H^+ \rightarrow t\bar{b}$ [53] for $\tan \beta < 2$ and $H \rightarrow \tau\tau$ [54] for $\tan \beta > 6$). All other constraints ($S, T, \text{HiggsSignals}, \text{SuperIso}$ and theoretical ones) are also checked.

In Fig. 4, we display the cumulative \mathcal{BR} s of the of the B state into SM particles (left panel) and non-SM particles (right panel), plotted as functions of the singlet bottom mass m_B and the parameter $\tan \beta$. It is evident that, for high values of $\tan \beta$, the decay rates into non-SM particles increase significantly, reaching up to 50% (38% within the permissible region). In contrast, at medium and low $\tan \beta$ values, regardless of m_B , the scenario reverses, with decays into SM particles becoming fully predominant.

Given this context, we propose three Benchmark Points (BPs) tailored for investigating the Type-II 2HDM extended by a singlet VLQ carrying the bottom EM charge. The proposed BPs are as follows⁷:

- i) BP₁: where $\mathcal{BR}(B \rightarrow \text{SM})$ is similar to $\mathcal{BR}(B \rightarrow \text{non SM})$;
- ii) BP₂: where $\mathcal{BR}(B \rightarrow \text{SM})$ is rather small, which makes $\mathcal{BR}(B \rightarrow \text{non SM})$ substantial;
- iii) BP₃: where $\mathcal{BR}(B \rightarrow \text{SM})$ is rather large, which makes $\mathcal{BR}(B \rightarrow \text{non SM})$ marginal.

Input parameters for these BPs are given in Tab. 2.

Parameters	BP ₁	BP ₂
Masses are in GeV		
m_h	125	125
m_H	645.79	774.80
m_A	406.54	754.38
m_{H^\pm}	677.91	786.51
$\tan \beta$	1.04	1.51
m_B	1946.63	1049.94
$\sin(\theta^d)_L$	0.061	-0.023
$\mathcal{BR}(H^\pm \rightarrow XY)$ in %		
$\mathcal{BR}(H^+ \rightarrow tb)$	54.31	99.80
$\mathcal{BR}(H^+ \rightarrow \tau\nu)$	0.00	0.0243
$\mathcal{BR}(H^+ \rightarrow W^+A)$	45.58	0.00
$\mathcal{BR}(B \rightarrow XY)$ in %		
$\mathcal{BR}(B \rightarrow W^+t)$	27.41	41.13
$\mathcal{BR}(B \rightarrow Zb)$	13.98	22.31
$\mathcal{BR}(B \rightarrow hb)$	13.86	21.69
$\mathcal{BR}(B \rightarrow Hb)$	11.07	4.62
$\mathcal{BR}(B \rightarrow Ab)$	12.78	5.22
$\mathcal{BR}(B \rightarrow H^-t)$	20.86	5.00
Γ in GeV		
$\Gamma(B)$	32.33	27.33

Table 2: The full description of our BPs for the (B) singlet case.

⁷Should these conditions not be fully satisfied, we will proceed with only two BPs instead of the proposed three.

3.2 2HDM with (TB) doublet

We now discuss the case of the (TB) doublet. In the SM extended with such a VLQ multiplet, both mixing angles in the up- and down-type quark sectors enter the phenomenology of the model⁸. For given θ_R^b , θ_R^t and m_B mass, the relationship between the mass eigenstates and the mixing angles reads as [8]:

$$m_T^2 = (m_B^2 \cos^2 \theta_R^b + m_b^2 \sin^2 \theta_R^b - m_t^2 \sin^2 \theta_R^t) / \cos^2 \theta_R^t, \quad (15)$$

from where one can compute the m_T value. Furthermore, using Eqs. (8)–(9), one can also compute the left mixing θ_L^b and θ_L^t .

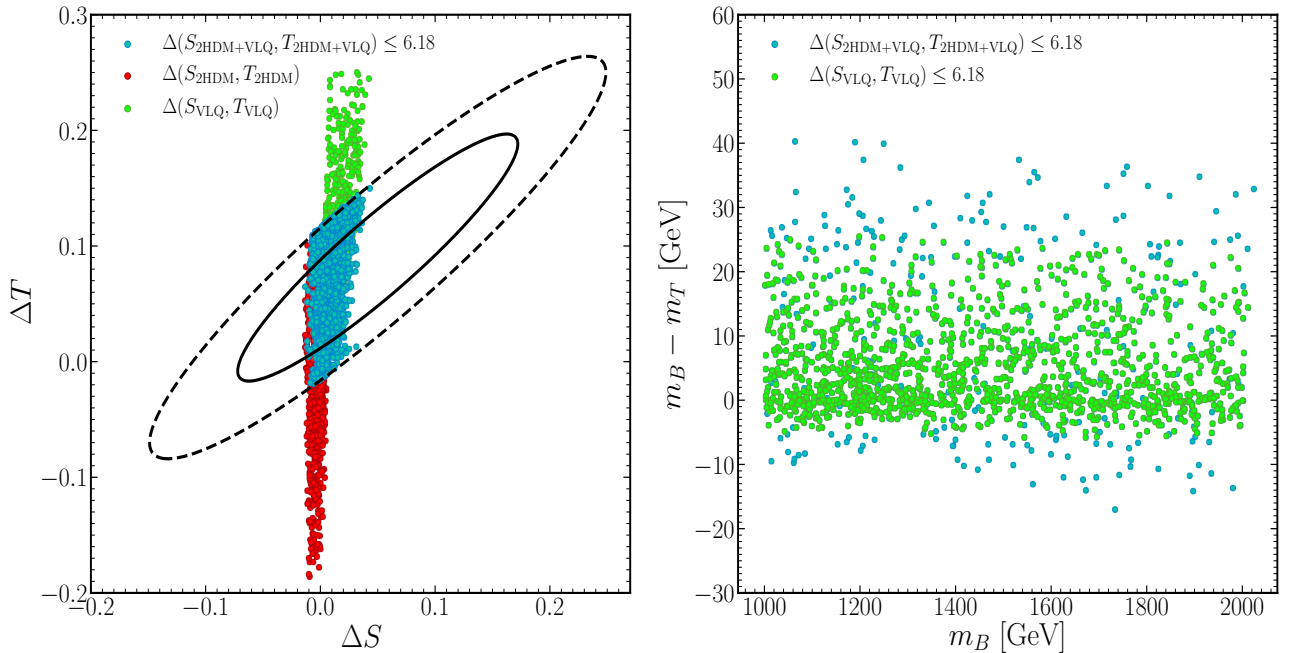


Figure 5: (Left) Scatter plots of randomly generated points superimposed onto the fit limits in the $(\Delta S, \Delta T)$ plane from EWPO data at 95% CL with a correlation of 92%. Here, we illustrate the 2HDM and VLQ contributions separately and also the total one. (Right) The same points are mapped onto the (m_B, δ) plane, where δ is the mass difference between B and T . Here, we only present the VLQ contribution and the total one. Further, all constraints have been taken into account.

In our analysis of the 2HDM+ (TB) doublet, we use the scan ranges described in Tab. 1. Fig. 5 depicts the S and T parameters, distinguishing the contributions from the VLQ and the 2HDM separately. As seen in the left panel of Fig. 5, similar to the earlier case involving a heavy bottom (B) singlet, the VLQ (TB) doublet and 2HDM states can contribute with opposite signs to the oblique parameters. This aspect could significantly alter the constraints on the 2HDM+VLQ parameter space derived from EWPOs. Moreover, as illustrated in the right panel of the same figure, within the SM extended by a VLQ (green points), the mass splitting between B and T must not exceed 25 GeV in the positive direction and 5 GeV in the negative direction. However, when introducing 2HDM states alongside VLQs, this allowed mass splitting widens, reaching up to 40 GeV positively and 10 GeV negatively.

⁸Hereafter, we replace the d and u superscripts in the mixing angles with b and t , respectively.

In the scenario of the SM extended by a VLQ (TB) doublet, the B state can decay through multiple modes: $B \rightarrow W^+t, Zb, th$. Notably, if the mixing angle θ_R^b is zero ($\theta_R^b = 0$), the bBZ and bBh couplings disappear, leading to a dominant decay mode of $B \rightarrow W^-t$. With non-zero mixing, these decay modes become viable, with their \mathcal{BR} s depending on the mixing angles and VLQ masses. The introduction of additional Higgs particles opens new decay channels: $B \rightarrow Ab, Hb, H^-t$ ⁹.

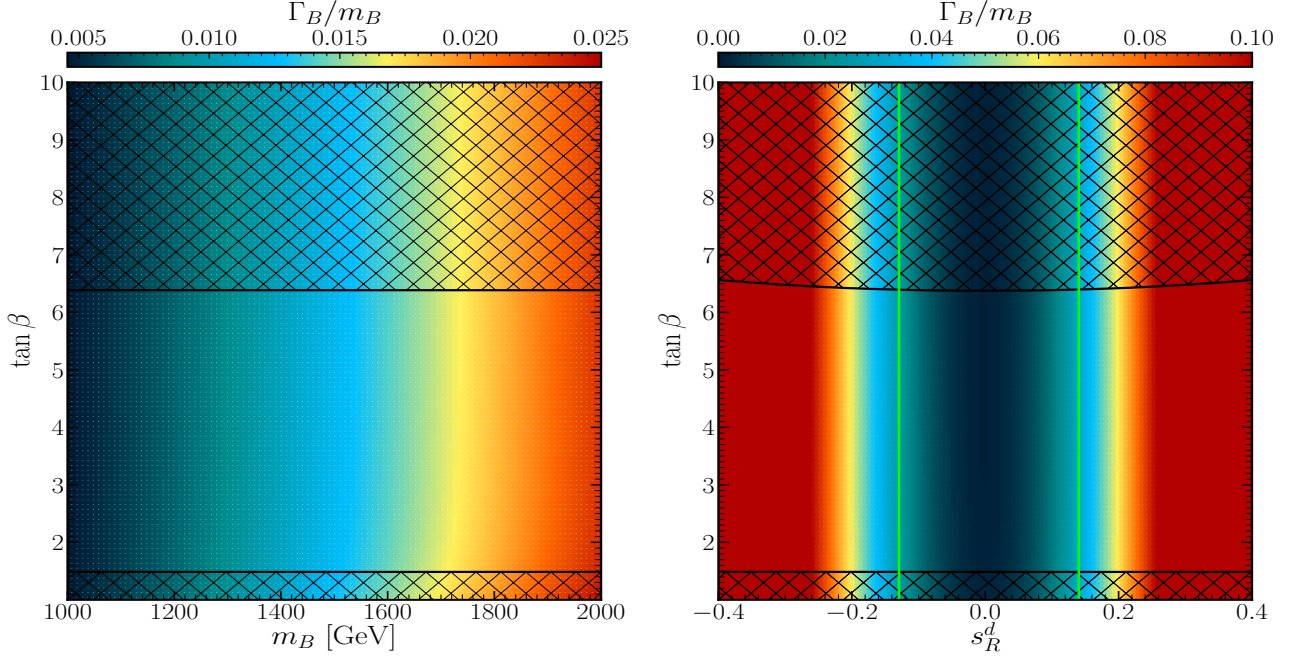


Figure 6: The $\Gamma(B)/m_B$ ratio ($\Gamma(B)$ mapped over the $(m_B, \tan \beta)$ plane (left) and $(s_R^d \equiv \sin \theta_R^d, \tan \beta)$ plane (right), with $\sin \theta_R^u = 0.042$ in the left panel and $m_B = 1600$ GeV in the right panel (the 2HDM parameters are the same as in Fig. 4). Here, the shaded areas are excluded by `HiggsBounds`. The regions between the vertical lime green lines are allowed by the S, T parameter constraints, all other constraints (`HiggsSignals`, `SuperIso` and theoretical ones) are also checked.

⁹It is crucial to consider that constraints on the mass splitting between B and T , as imposed by the S and T parameters, restrict the potential for VLQ decays into each other, such as $B \rightarrow W^-/H^-T$. Therefore, we will concentrate solely on the kinematically open $1 \rightarrow 2$ channels (on-shell decays).

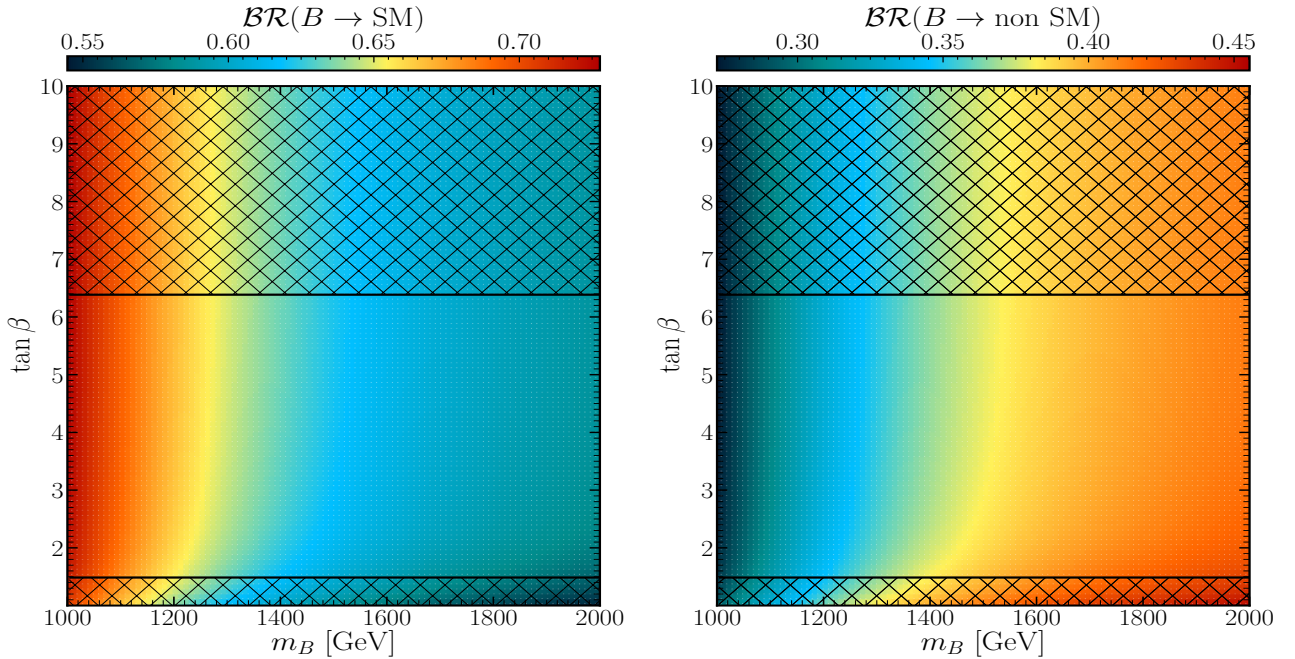


Figure 7: The $\mathcal{BR}(B \rightarrow \text{SM})$ (left) and $\mathcal{BR}(B \rightarrow \text{non SM})$ (right) mapped onto the $(m_B, \tan \beta)$ plane, with the same description as in Fig. 6 (left).

To further explore the phenomenology of this BSM setup, we perform a comprehensive scan over both the 2HDM and VLQ (TB) doublet parameters as specified in Tab. 1, adhering to all theoretical and experimental constraints. Fig. 6 displays the total width of the B state as a function of its mass m_B (left panel) and the down-quark sector mixing angle s_R^d (right panel), with both dimensions correlated to m_B and showing insensitivity to $\tan \beta$. The analysis reveals that $\Gamma(B)/m_B$ significantly increases with m_B , and, as indicated in the right panel, this trend is particularly pronounced for large mixing values ($|s_R^d| \geq 2$) which are already beyond the permissible bounds set by the S and T parameters (green line).

Fig. 7 explores the decay patterns into SM and non-SM particles, the latter involving one additional Higgs state, such as $B \rightarrow tH^-$, $B \rightarrow Ab$ and $B \rightarrow Hb$ ¹⁰. This analysis reveals that non-SM decay channels of the B state can account for up to 40% of decays for higher m_B values, with negligible dependence on $\tan \beta$.

¹⁰In principle, in the definition of these two \mathcal{BR} s, one should account for the $B \rightarrow W^-T$ and $B \rightarrow H^-T$ decays, however, because both the W^- and H^- are off-shell, they are always small, so we will not discuss these here (recall the degeneracy $m_B \sim m_T$).

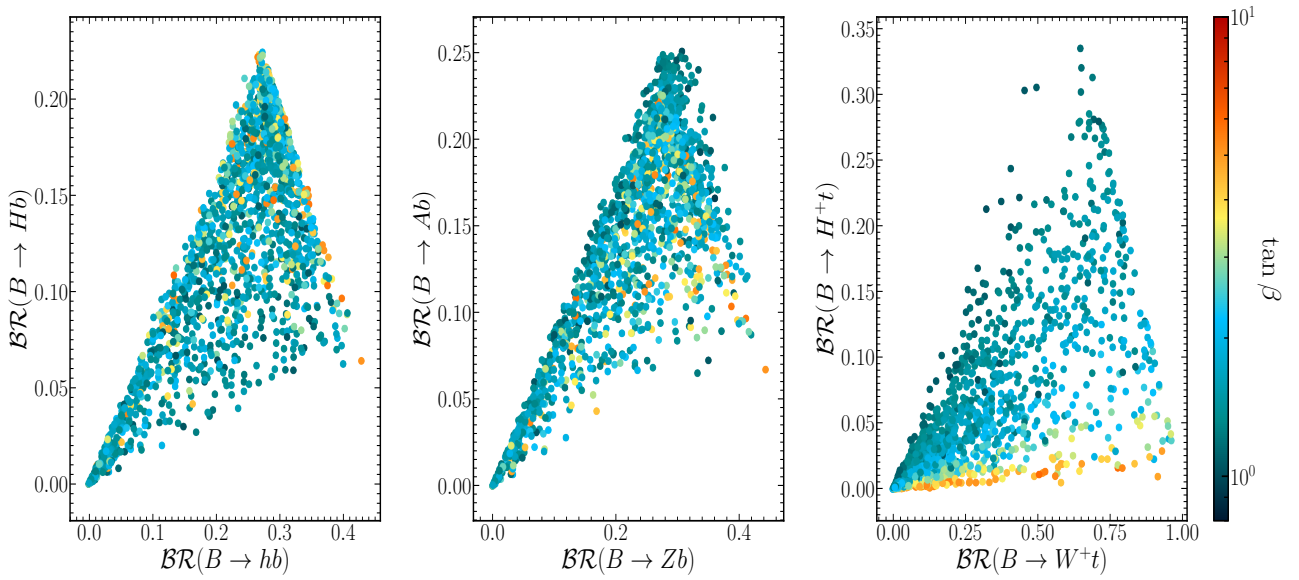


Figure 8: The correlation between $\mathcal{BR}(B \rightarrow hb)$ and $\mathcal{BR}(B \rightarrow Hb)$ (left), $\mathcal{BR}(B \rightarrow Zb)$ and $\mathcal{BR}(B \rightarrow Ab)$ (middle) as well as $\mathcal{BR}(B \rightarrow W^-t)$ and $\mathcal{BR}(B \rightarrow H^-t)$ (right) with $\tan\beta$ indicated in the color gauge.

In Fig. 8, we further analyze the correlation between the individual SM and non-SM decay channels of the B state. This examination reveals that, across both neutral and charged current scenarios, non-SM decay channels generally exhibit lower \mathcal{BR} s compared to their SM ones. Specifically, the \mathcal{BR} for $B \rightarrow Zb$ and $B \rightarrow hb$ can reach approximately 45% while for $B \rightarrow Ab$ and $B \rightarrow Hb$ can touch around 25% at most. Furthermore, the analysis indicates a notable variation in the charged current decays: the non-SM decay $B \rightarrow H^-t$ can achieve a maximum \mathcal{BR} of 34% at low $\tan\beta$ values. In contrast, the SM decay $B \rightarrow W^-t$ can reach up to 100% at medium $\tan\beta$ levels. This discrepancy highlights the impact of $\tan\beta$ on the decay behavior of the B state, with the couplings bBH and bBA showing a slight increase proportional to $\tan\beta$ at medium levels of this parameter.

Parameters	BP ₁	BP ₂
Masses are in GeV		
m_h	125	125
m_H	598.48	700.23
m_A	449.60	470.00
m_{H^\pm}	613.8	685.86
$\tan \beta$	1.79	1.17
m_T	1898.63	1071.66
m_B	1916.73	1068.72
$\sin(\theta^u)_L$	-0.000059	0.012241
$\sin(\theta^d)_L$	0.000345	-0.000047
$\sin(\theta^u)_R$	-0.000653	0.075789
$\sin(\theta^d)_R$	0.137099	-0.010480
$\mathcal{BR}(H^\pm \rightarrow XY)$ in %		
$\mathcal{BR}(H^+ \rightarrow tb)$	62.73	63.8
$\mathcal{BR}(H^+ \rightarrow W^+A)$	37.13	36.08
$\mathcal{BR}(B \rightarrow XY)$ in %		
$\mathcal{BR}(B \rightarrow W^-t)$	0.0017	79.11
$\mathcal{BR}(B \rightarrow W^-T)$	-	-
$\mathcal{BR}(B \rightarrow Zb)$	27.03	0.79
$\mathcal{BR}(B \rightarrow hb)$	26.80	0.77
$\mathcal{BR}(B \rightarrow Hb)$	22.01	0.26
$\mathcal{BR}(B \rightarrow Ab)$	24.14	0.52
$\mathcal{BR}(B \rightarrow H^-t)$	0.00	18.53
$\mathcal{BR}(B \rightarrow H^-T)$	-	-
Γ in GeV		
$\Gamma(B)$	78.82	2.75

Table 3: The full description of our BPs for the (TB) doublet case.

Building on the approach of the previous section, we conclude this part by introducing in Tab. 3 two BPs that are conducive to experimental exploration. These BPs are designed with a focus on B quark masses and feature varying widths (Γ_B) to span a range of possible detection scenarios.

3.3 2HDM with (BY) doublet

In the case of the SM extended with a (BY) doublet, the ensuing VLQ structure is fully described by the θ_R^b mixing angle and the new bottom mass m_B . In fact, for a given θ_R^b value, θ_L^b is computed using Eq. (9). The mass of the new VLQ with exotic EM charge $(+5/3)$, the Y state, is given as a function of such a mixing angle m_B as well as m_b by [8].

$$m_Y^2 = m_B^2 \cos^2 \theta_R^2 + m_b^2 \sin^2 \theta_R^2. \quad (16)$$

This is independent (at tree level) from the additional parameters entering the 2HDM Higgs sector, however, the latter impinges on the viability of this BSM construct against EWPO data.

Expanding on the analysis presented in Tab. 1, Fig. 9 (left) shows that while the combined (VLQ+2HDM) contribution is within the 2σ CL of the ΔS and ΔT parameters (blue points), the two separate contributions from the VLQ and 2HDM sectors frequently surpass the boundaries established by EWPO data ellipses.

In the right panel of Fig. 9, we further illustrate the size of the mass splitting $\delta = m_B - m_Y$ allowed by EWPO data. In the case of the VLQ only structure, the splitting is always very small. Instead, in the case of the full 2HDM+VLQ scenario, one can see that the splitting could be very large, of the order of 40 GeV, the more so the larger m_B .

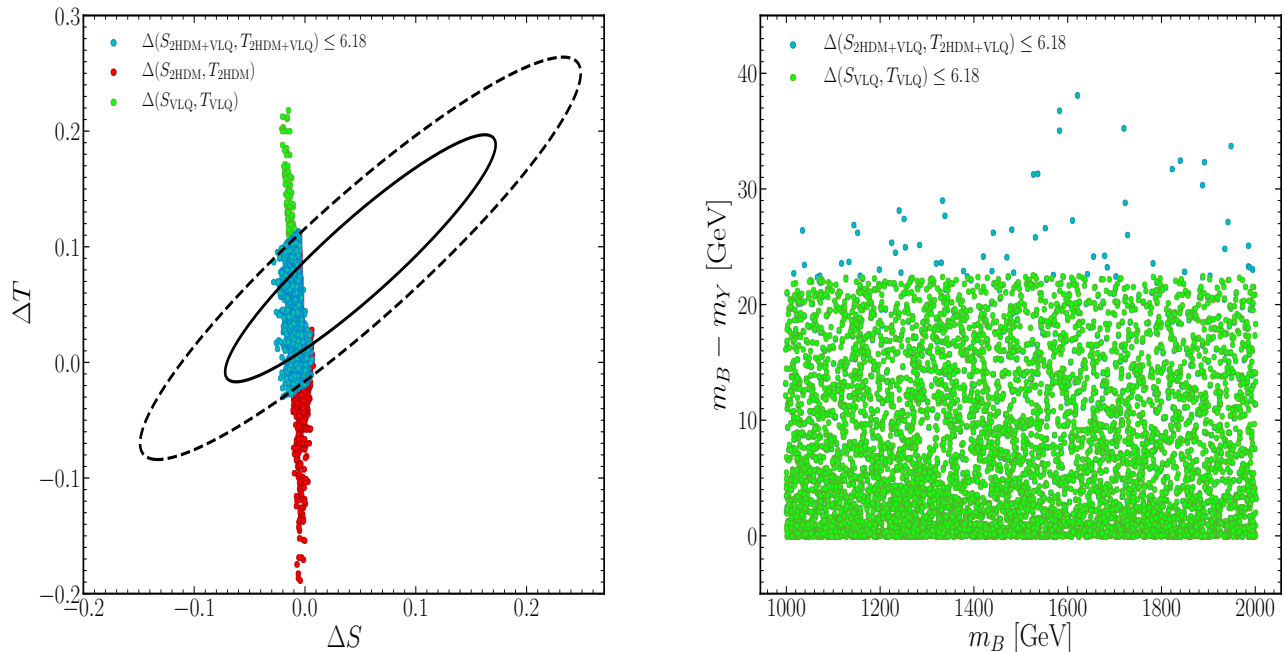


Figure 9: (Left) Scatter plots of randomly generated points superimposed onto the fit limits in the $(\Delta S, \Delta T)$ plane from EWPO data at 95% CL with a correlation of 92%. Here, we illustrate the 2HDM and VLQ contributions separately and also the total one. (Right) The same points are here mapped onto the (m_B, δ) plane, where δ is the mass difference between B and Y . Here, we only present the VLQ contribution and the total one. Further, all constraints have been taken into account.

In Fig. 10, we compare again $\mathcal{BR}(B \rightarrow \text{SM})$ to $\mathcal{BR}(B \rightarrow \text{non SM})$, mapped over m_B and $\tan \beta$. In contrast to the previous VLQ doublet realization, here, the non-SM decays of the B state can dominate, potentially reaching up to 100% within the permissible parameter space, which notably expands with increasing $\tan \beta$. Interestingly, the decay behavior of the heavy bottom partner shows minimal sensitivity to the mass m_B .

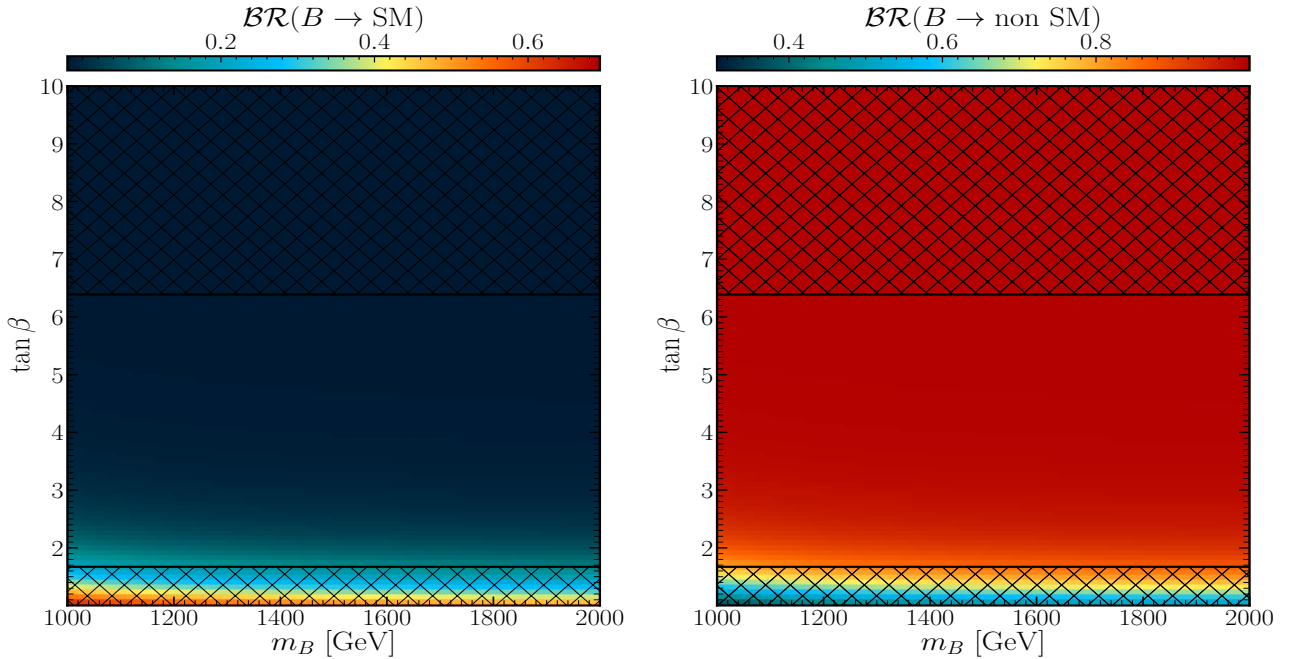


Figure 10: The $\mathcal{BR}(B \rightarrow \text{SM})$ (left) and $\mathcal{BR}(B \rightarrow \text{non SM})$ (right) mapped onto the $(m_B, \tan \beta)$ plane, with $\sin \theta_R^u = 0.057$ (the 2HDM parameters are the same as in Fig. 4). Here, the shaded areas are excluded by HiggsBounds, and all other constraints (S , T , HiggsSignals, SuperIso and theoretical ones) are also checked.

We now discuss the size of the individual \mathcal{BR} s of B decays. As usual, alongside the SM decays of new bottom B , into W^-t, Zb and hb , one only has the non-SM decays $B \rightarrow Hb$ and $B \rightarrow Ab$: in fact, the $B \rightarrow H^-t$ channel is not available, as the intervening coupling is identically zero, hence it is excluded from our discussion.

In Fig. 11, we present the usual correlations between $\mathcal{BR}(B \rightarrow hb)$ and $\mathcal{BR}(B \rightarrow Hb)$ (left) as well as $\mathcal{BR}(B \rightarrow Zb)$ and $\mathcal{BR}(B \rightarrow Ab)$ (right). At medium $\tan \beta$ values (noting that large $\tan \beta$ values are ruled out by $H \rightarrow \tau\tau$ [54] searches), $\mathcal{BR}(B \rightarrow Hb)$ and $\mathcal{BR}(B \rightarrow Ab)$ significantly rise, each reaching up to 50% as their respective couplings increase proportionally to $\tan \beta$. This results in a notable elevation of $\mathcal{BR}(B \rightarrow Zb)$ and $\mathcal{BR}(B \rightarrow hb)$, positioning medium $\tan \beta$ as an ideal range for investigating exotic B decays within the established parameter space. Conversely, at lower $\tan \beta$ values, $\mathcal{BR}(B \rightarrow hb)$ and $\mathcal{BR}(B \rightarrow Zb)$ receive a boost, each approaching approximately 38%, which in turn mildly suppresses $\mathcal{BR}(B \rightarrow Hb)$ and $\mathcal{BR}(B \rightarrow Ab)$. This nuanced behavior across different $\tan \beta$ ranges underscores the complex interplay between these parameters and the decay modes of the B state in this BSM framework. At small $\tan \beta$, instead, one can see that both $\mathcal{BR}(B \rightarrow hb)$ and $\mathcal{BR}(B \rightarrow Zb)$ are somewhat enhanced with each nearing 38% and therefore $\mathcal{BR}(B \rightarrow Hb)$ and $\mathcal{BR}(B \rightarrow Ab)$ are somewhat suppressed.

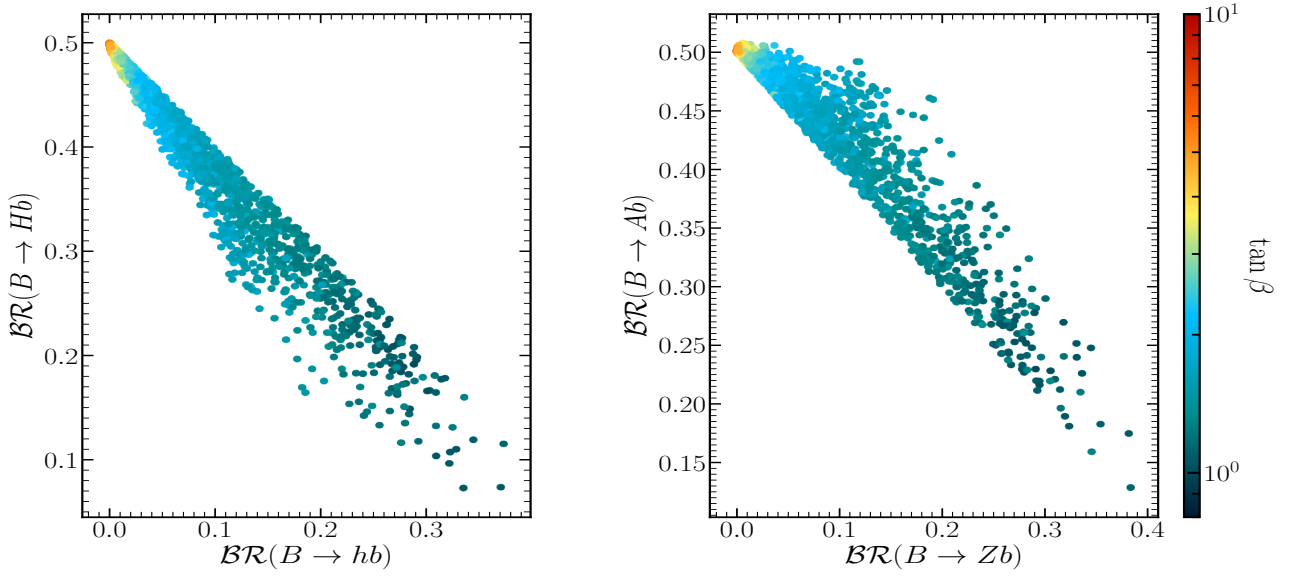


Figure 11: The correlation between $\mathcal{BR}(B \rightarrow hb)$ and $\mathcal{BR}(B \rightarrow Hb)$ (left), $\mathcal{BR}(B \rightarrow Zb)$ and $\mathcal{BR}(B \rightarrow Ab)$ (right) with $\tan \beta$ as indicated in the color gauge.

Parameters	BP ₁	BP ₂	BP ₃
Masses are in GeV			
m_h	125	125	125
m_H	710.03	608.02	782.90
m_A	629.51	604.74	765.13
m_{H^\pm}	748.28	602.00	773.11
$\tan \beta$	1.17	5.94	1.12
m_B	1266.05	1686.13	1042.89
m_Y	1262.22	1686.10	1040.30
$\sin(\theta^d)_L$	0.000294	0.000018	-0.000324
$\sin(\theta^d)_R$	0.077721	0.006235	-0.070470
$\mathcal{BR}(H^\pm \rightarrow XY)$ in %			
$\mathcal{BR}(H^+ \rightarrow tb)$	94.54	95.74	99.82
$\mathcal{BR}(H^+ \rightarrow \tau\nu)$	0.00	4.06	4.5000
$\mathcal{BR}(H^+ \rightarrow W^+A)$	5.28	0.00	0.00
$\mathcal{BR}(B \rightarrow XY)$ in %			
$\mathcal{BR}(B \rightarrow W^-t)$	0.00	0.00	0.0015
$\mathcal{BR}(B \rightarrow W^-T)$	-	-	-
$\mathcal{BR}(B \rightarrow Zb)$	25.24	0.05	38.34
$\mathcal{BR}(B \rightarrow hb)$	24.75	0.05	37.26
$\mathcal{BR}(B \rightarrow Hb)$	22.67	49.86	11.50
$\mathcal{BR}(B \rightarrow Ab)$	27.33	50.02	12.87
$\mathcal{BR}(B \rightarrow H^-t)$	-	-	-
$\mathcal{BR}(B \rightarrow H^-T)$	-	-	-
Γ in GeV			
$\Gamma(B)$	7.92	57.94	2.397

Table 4: The full description of our BPs for the (BY) doublet case.

Concluding our discussion, for further exploration of this BSM scenario, we propose three BPs as detailed in Tab. 4. These BPs encapsulate the conditions elucidated earlier.

3.4 2HDM with (XTB) triplet

We discuss here the (XTB) triplet case. Before presenting our numerical results, though, let us first introduce our parametrization. This model is fixed by giving the new bottom mass and one mixing angle, let us say θ_L^t , the other parameters are then computable. In fact, θ_R^t is derived from Eq. (9) while m_X is given by [8]:

$$m_X^2 = m_T^2 \cos^2 \theta_L^u + m_t^2 \sin^2 \theta_L^u = m_B^2 \cos^2 \theta_L^b + m_b^2 \sin^2 \theta_L^b. \quad (17)$$

Using the above relation between m_T and m_X together with the one between up- and down-type quark mixing in Eq. (10), one can derive the mass of the new bottom quark as follows:

$$m_B^2 = \frac{1}{2} \sin^2(2\theta_L^u) (m_T^2 - m_t^2)^2 / (m_X^2 - m_b^2) + m_X^2. \quad (18)$$

The down-type quark mixing is then given by.

$$\sin(2\theta_L^d) = \sqrt{2} \frac{m_T^2 - m_t^2}{m_B^2 - m_b^2} \sin(2\theta_L^u). \quad (19)$$

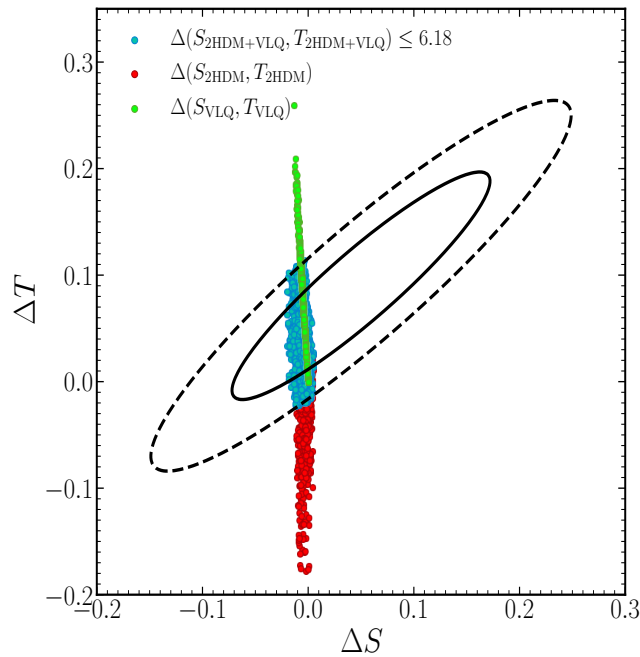


Figure 12: Scatter plots for randomly generated points superimposed onto the fit limits in the $(\Delta S, \Delta T)$ plane from EWPO data at 95% CL with a correlation of 92%. Here, we illustrate the 2HDM and VLQ contributions separately and also the total one. Further, all constraints have been taken into account.

As usual, we conduct a systematic scan over the parameters of both the 2HDM and VLQ sectors, as detailed in Tab. 1. In Fig. 12, it is evident that, while the combined contribution of 2HDM and VLQ falls within the 95% CL of $\Delta\chi^2$ for ΔS and ΔT , the individual contributions of 2HDM and VLQ origin mostly lie outside the 2σ level.

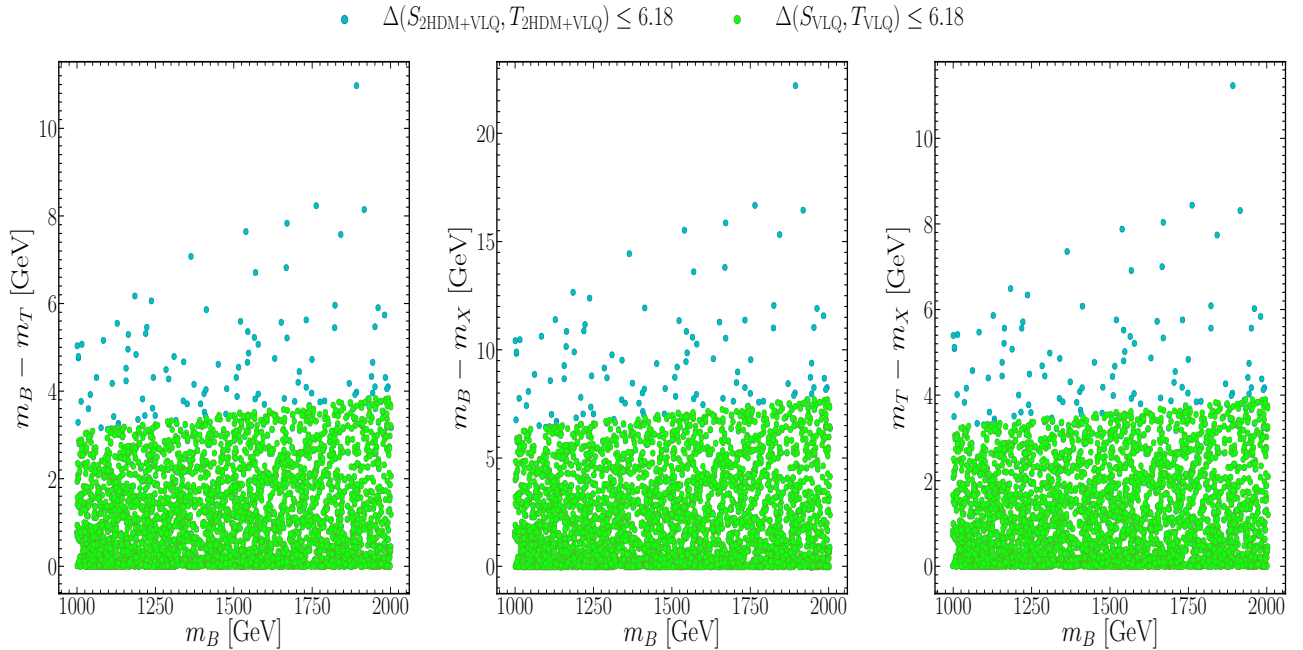


Figure 13: Scatter plots of randomly generated points mapped onto the (m_B, δ) plane, where δ is the mass difference between B and T , B and X , and T and X . Here, we illustrate the VLQ and 2HDM+VLQ contributions separately. Further, all constraints have been taken into account.

Furthermore, the splitting between m_B , m_T and m_X is severely constrained by the EWPOs, as depicted in Fig. 13, where mass differences mapped against m_B are given. It is noticeable that such a splitting is relatively small in the case of the SM with a VLQ construct, approximately of the order of a few GeV. However, in the case of the full 2HDM with VLQ scenario, such a splitting becomes significantly larger, reaching up to 11 or 22 GeV, indicating that inter VLQ decays are likely to play a negligible role in this BSM realization.

Regarding the 2HDM with a (XTB) triplet, the VLB can decay into the SM channels (Zb , hb and W^-t) as well as extra channels Hb , Ab , H^-t involving additional Higgs states of the 2HDM. The relative importance of these channels is depicted in Fig. 14, revealing the dominance of non-SM channels, particularly evident at medium $\tan\beta$ values where it can reach 100%. However, SM channels can still contribute significantly, reaching up to 60% in cumulative branching ratios within the allowed range. Now, we proceed to discuss these individual B decay channels. (Note that, due to the small splitting between X and B , the decay $B \rightarrow W^-Y$ is closed for a real W^- and is highly suppressed for an off-shell one, so we do not discuss it here.)

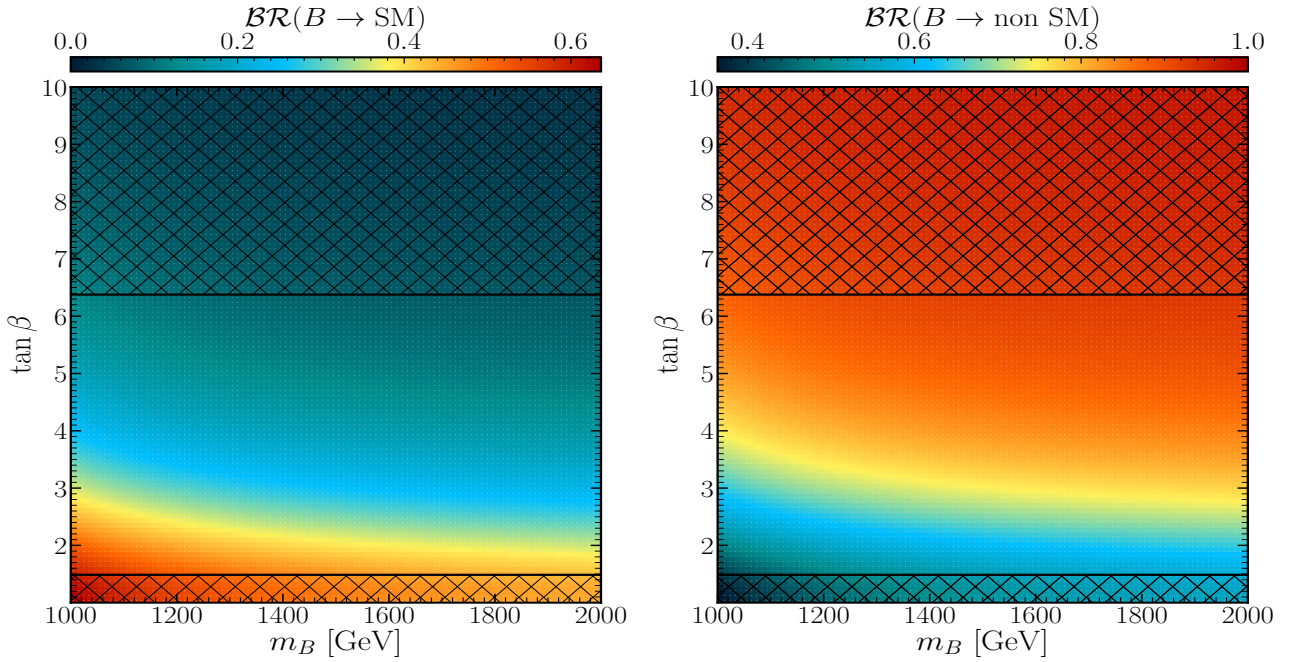


Figure 14: The $\mathcal{BR}(B \rightarrow \text{SM})$ (left) and $\mathcal{BR}(B \rightarrow \text{non SM})$ (right) mapped onto the $(m_B, \tan \beta)$ plane, with $\sin \theta_L^u = 0.0093$ (the 2HDM parameters are the same as in Fig. 4). Here, the shaded areas are excluded by HiggsBounds, and all other constraints (S , T , HiggsSignals, SuperIso and theoretical ones) are also checked.

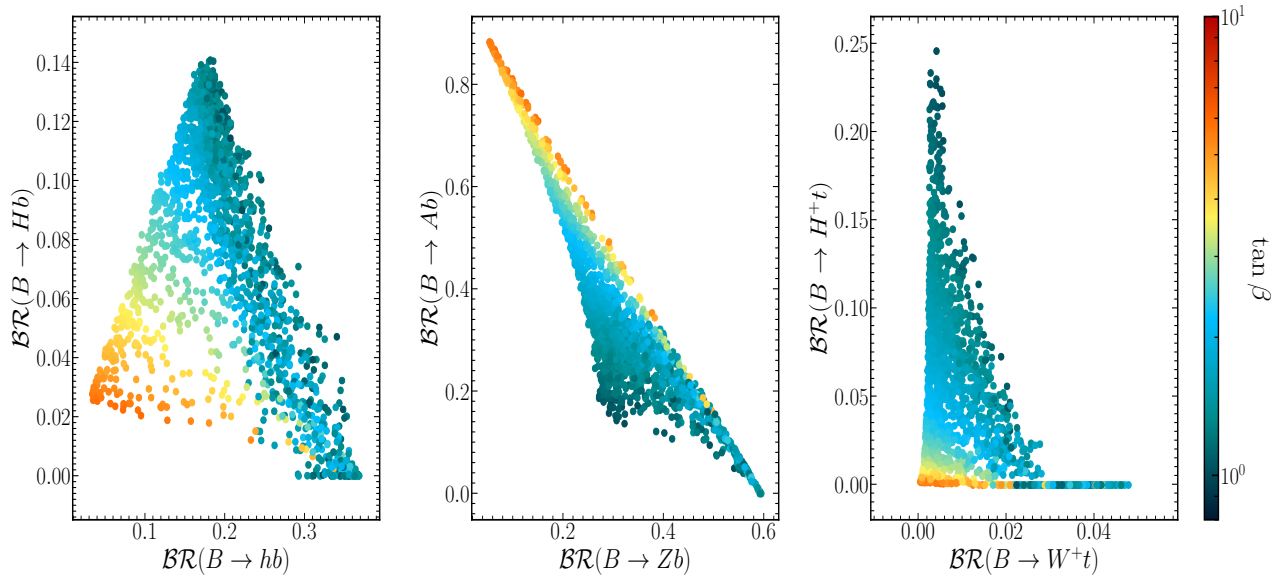


Figure 15: The correlation between $\mathcal{BR}(B \rightarrow hb)$ and $\mathcal{BR}(B \rightarrow Hb)$ (left), $\mathcal{BR}(B \rightarrow Zb)$ and $\mathcal{BR}(B \rightarrow Ab)$ (middle) as well as $\mathcal{BR}(B \rightarrow W^+t)$ and $\mathcal{BR}(B \rightarrow H^+t)$ (right) with $\tan \beta$ indicated in the color gauge.

As previously mentioned, the introduction of additional channels associated with the extra 2HDM states has implications for the SM framework. While the SM predicts the decay of the new bottom quark into final states, such as Zb, hb and W^-t , the full 2HDM+VLQ scenario introduces new channels $B \rightarrow Hb, Ab, H^-t$ that could be of significant importance and in the present multiplet structure. Specifically, the decay $B \rightarrow Ab$ could exhibit a \mathcal{BR} as high as 90% for large $\tan \beta$ values, owing to its coupling proportionality to $\tan \beta$. In contrast, the relevance

of other exotic decays is limited, typically reaching up to 25%. These patterns are illustrated in Fig. 15.

Once again, we offer an overview of our proposed BPs in Tab. 5, all of which meet the conditions discussed previously.

Parameters	BP ₃	BP ₂	BP ₁
Masses are in GeV			
m_h	125	125	125
m_H	782.99	630.00	599.77
m_A	719.97	629.92	586.59
m_{H^\pm}	788.20	686.76	602.36
$\tan \beta$	1.23	5.64	2.08
m_T	1024.61	1833.36	1022.66
m_B	1024.98	1833.60	1022.69
m_X	1024.2	1833.12	1022.64
$\sin(\theta^u)_L$	0.028	-0.016	0.0071
$\sin(\theta^d)_L$	0.038	-0.022	0.0097
$\mathcal{BR}(H^\pm \rightarrow XY)$ in %			
$\mathcal{BR}(H^+ \rightarrow tb)$	99.80	96.19	99.73
$\mathcal{BR}(H^+ \rightarrow \tau\nu)$	0.011	3.45	0.08
$\mathcal{BR}(H^+ \rightarrow W^+A)$	0.014	0.07	0.00
$\mathcal{BR}(B \rightarrow XY)$ in %			
$\mathcal{BR}(B \rightarrow W^+t)$	1.72	0.06	1.10
$\mathcal{BR}(B \rightarrow W^+T)$	-	-	-
$\mathcal{BR}(B \rightarrow Zb)$	46.64	5.43	29.89
$\mathcal{BR}(B \rightarrow hb)$	29.55	3.51	18.94
$\mathcal{BR}(B \rightarrow Hb)$	5.28	2.75	8.40
$\mathcal{BR}(B \rightarrow Ab)$	11.93	88.06	38.00
$\mathcal{BR}(B \rightarrow H^+t)$	4.86	0.16	3.64
$\mathcal{BR}(B \rightarrow H^+T)$	-	-	-
Γ in GeV			
$\Gamma(B)$	0.85	15.000	0.086

Table 5: The full description of our BPs for the (XTB) triplet case.

3.5 2HDM with (TBY) triplet

We finally discuss the (TBY) triplet case. In the 2HDM with such a VLQ representation, the situation is very similar to the case of the (T) singlet and (TB) doublet. Before discussing our numerical results, though, let us again first introduce our parametrization. This model is fixed by giving the new top mass and one mixing angle, let us say θ_L^t , the other parameters are then computable. In fact, θ_R^t is derived from Eq. (9) while m_Y is given by [8]:

$$m_Y^2 = m_T^2 \cos^2 \theta_L^t + m_t^2 \sin^2 \theta_L^t = m_B^2 \cos^2 \theta_L^b + m_b^2 \sin^2 \theta_L^b. \quad (20)$$

Using the above relation between m_T and m_Y together with the one between up- and down-type quark mixing in Eq. (10), one can derive the mass of the new bottom quark as:

$$m_B^2 = \frac{1}{8} \sin^2 2\theta_L^t \frac{(m_T^2 - m_t^2)^2}{m_Y^2 - m_b^2} + m_Y^2. \quad (21)$$

With this in hand, one can then derive the down-type quark mixing $\theta_{L,R}^d$ using Eqs. (9)–(10).

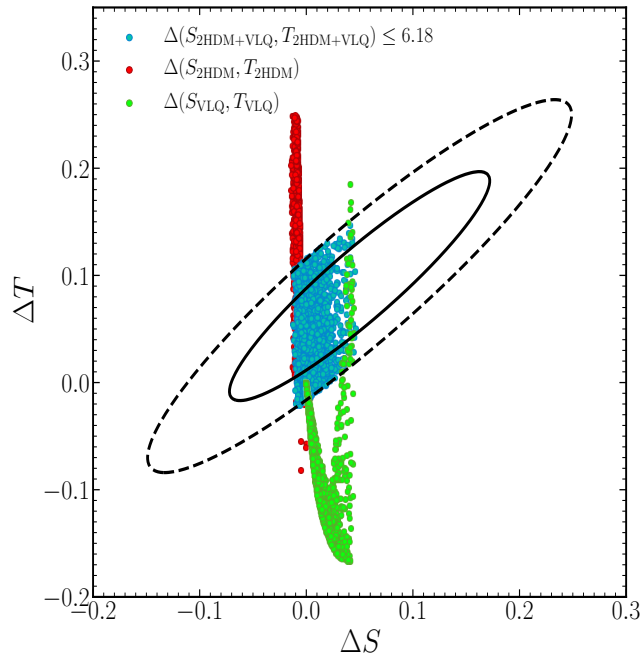


Figure 16: Scatter plots for randomly generated points superimposed onto the fit limits in the $(\Delta S, \Delta T)$ plane from EWPO data at 95% CL with a correlation of 92%. Here, we illustrate the 2HDM and VLQ contributions separately and also the total one. Further, all constraints have been taken into account.

Based on the scan listed in Tab. 1, we first illustrate in Fig. 16 the allowed 95% CL regions from the S and T parameter constraints, which shows that both the 2HDM only and VLQ only contributions could well be out of the allowed ranges but, when adding these together, one indeed finds viable solutions because of cancellations. As mentioned previously, when adding VLQs alongside extra Higgs states, the phenomenology of the S and T can change drastically, with respect to the SM case.

Following Fig. 17, in the SM with this considered VLQ representation, the splitting δ between the masses of T and B (left), T and Y (middle) as well as B and Y (right) is rather small, of the order a fraction of GeV at small m_T . However, for high m_T values, there exists a narrow strip of parameter space where these splittings could be of the order 1 GeV. This is very little. In contrast, in the 2HDM+VLQ scenario, the dynamics change significantly. The splitting between B and T could reach -15 GeV for small m_B (around 1000 GeV), while the splittings between B and Y , as well as T and Y , could extend up to 30 GeV in the same mass region. For large m_B , the mass splitting of both the individual contributions of VLQ and the combined 2HDM+VLQ scenario could reach up to -28 GeV between B and T , and up to -58 GeV between B and Y as well as T and Y . Once again, the significant cancellations between additional Higgs and VLQ states, naturally occurring in loop contributions due to their different spin statistics, enable the expansion of significant parameter space. This parameter space will be further explored in line with the analyses presented in the preceding two subsections to study 2HDM decays of VLQ states. Nonetheless, the small values of δ observed in these plots underscore the fact that VLQ decays into each other are once again mostly negligible.

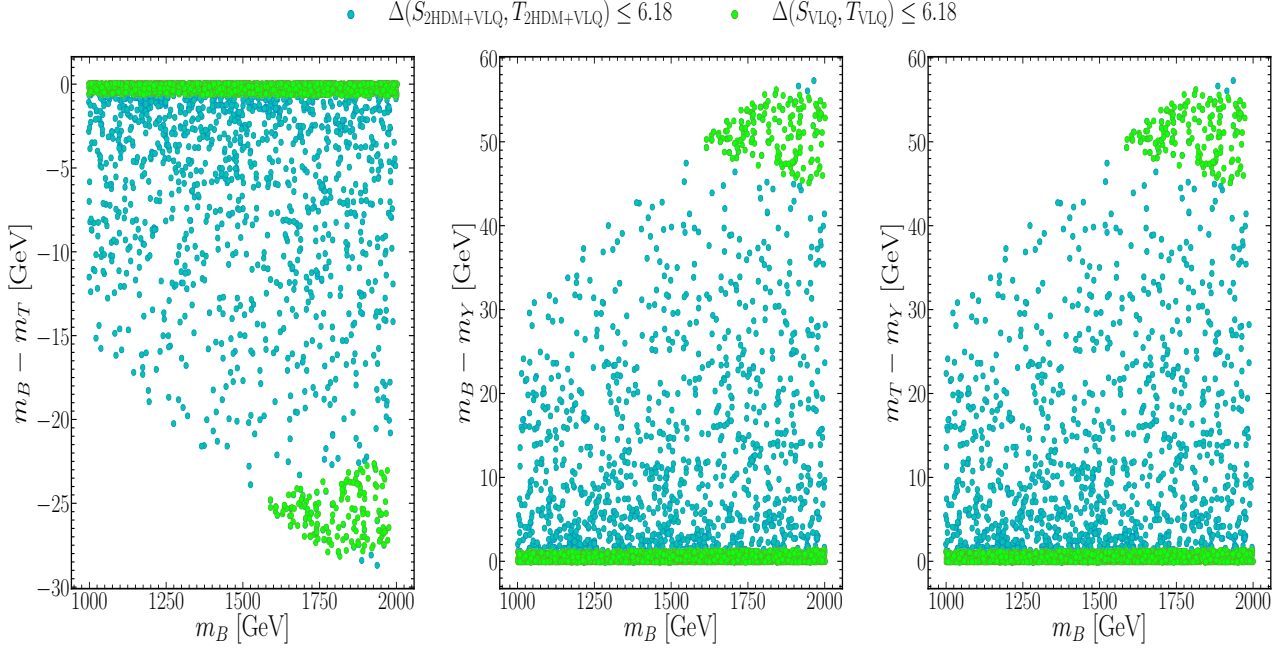


Figure 17: Scatter plots of randomly generated points mapped onto the $(m_{T/B}, \delta)$ plane, where δ is the mass difference between T and B , T and Y , and B and Y . Here, we illustrate the VLQ and 2HDM+VLQ contributions separately. Further, all constraints have been taken into account.

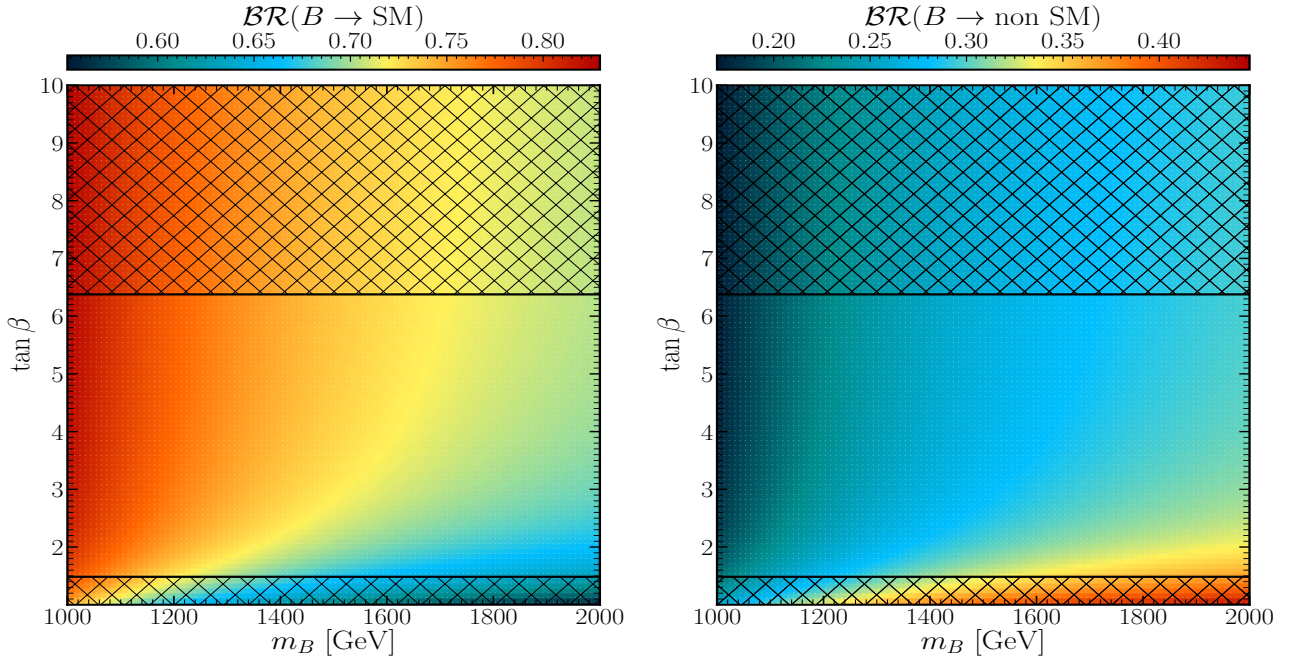


Figure 18: The $\mathcal{BR}(T \rightarrow \text{SM})$ (left) and $\mathcal{BR}(T \rightarrow \text{non SM})$ (right) mapped onto the $(m_T, \tan \beta)$ plane, with $\sin \theta_L^u = 0.02$ (the 2HDM parameters are the same as in Fig. 4). Here, the shaded areas are excluded by HiggsBounds, and all other constraints (S , T , HiggsSignals, SuperIso and theoretical ones) are also checked.

In the SM with a (TBY) triplet, the decay patterns of B states are essentially the same as in the (TB) doublet case. Therefore, in Fig. 18, we investigate the decays of the new bottom quark into both SM channels, such as Zb , hb and W^-t as well exotic ones, such as Hb , Ab and

H^-t . The cumulative \mathcal{BR} s of non-SM decays are notably pronounced, particularly evident at small $\tan\beta$ values and large m_B , where they can reach up to 35% within the allowed region. However, SM channels still dominate, accounting for approximately 80% of cumulative \mathcal{BR} s for small m_B values around 1000 GeV within the allowed range.

We move now on to delve into the individual B decay channels depicted in Fig. 19. important to note that, due to the small splitting between B and Y , the decay $B \rightarrow W^-Y$ is closed for a real W^- and highly suppressed for an off-shell one, thus we will not discuss it here. Clearly, one can observe from the figure a strong anti-correlation between standard and exotic channels. Regarding charged currents, the $\tan\beta$ dependence reveals that large values of it favor SM decays whereas small values favor 2HDM ones. Concerning neutral currents, both large and medium $\tan\beta$ values result in both the SM decays and 2HDM ones achieving their maximum, around 21% for the SM and 15% for the 2HDM.

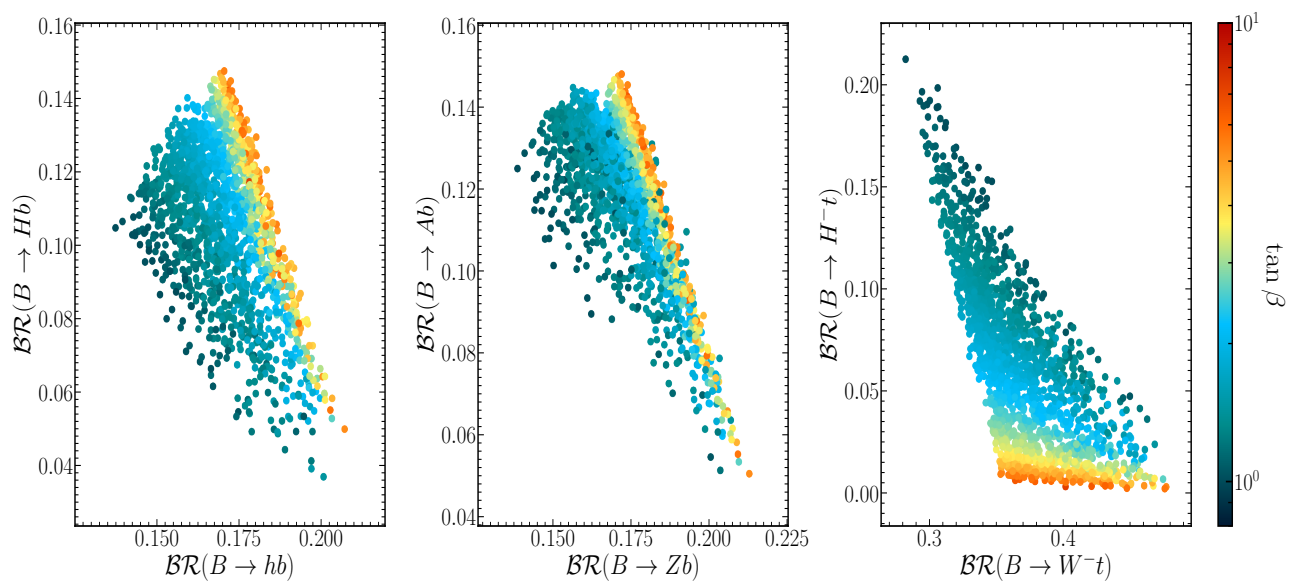


Figure 19: The correlation between $\mathcal{BR}(B \rightarrow hb)$ and $\mathcal{BR}(B \rightarrow Hb)$ (left) (right), $\mathcal{BR}(B \rightarrow Zb)$ and $\mathcal{BR}(B \rightarrow Ab)$ (middle) as well as $\mathcal{BR}(B \rightarrow W^-t)$ and $\mathcal{BR}(B \rightarrow H^-t)$ (left) with $\tan\beta$ indicated in the color gauge.

Proceeding to our BPs, we initially analyze the ratio $\Gamma(B)/m_B$ illustrated in Fig. 20. This visualization underscores the consistently narrow nature of the B state within our BSM framework. Notably, the quantity $\Gamma(B)/m_B$ reaches its peak of 0.008, primarily observed for high values of m_B . Subsequently, in Tab. 6, we present our BP explicitly, which include both light (BP₁) and heavy (BP₂) B states. This diverse selection allows for a comprehensive exploration of exotic B decays in phenomenological analyses.

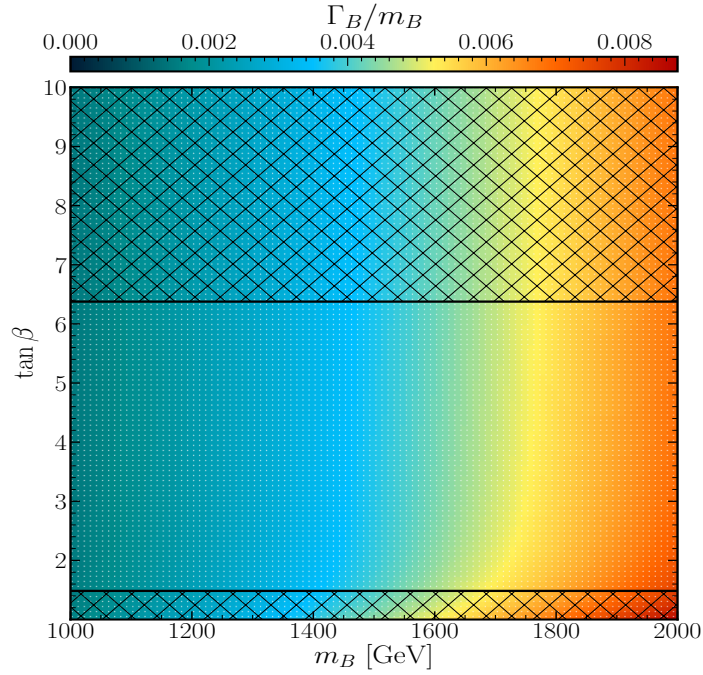


Figure 20: The ratio $\Gamma(B)/m_B$ mapped over the $(m_T, \tan \beta)$ plane. with $\sin \theta_L^u = 0.02$ (the 2HDM parameters are the same as in Fig. 4). Here, the shaded areas are excluded by HiggsBounds, and all other constraints (S , T , HiggsSignals, SuperIso and theoretical ones) are also checked.

Parameters	BP ₁	BP ₂
Masses are in GeV		
m_h	125	125
m_H	772.39	656.89
m_A	770.13	384.936
m_{H^\pm}	777.26	683.82
$\tan \beta$	5.22	1.04
m_T	1075.63	1813.76
m_B	1075.48	1809.04
m_Y	1075.33	1804.39
$\sin(\theta^u)_L$	-0.023	0.102
$\sin(\theta^d)_L$	-0.016	0.0716
$\mathcal{BR}(H^\pm \rightarrow XY)$ in %		
$\mathcal{BR}(H^+ \rightarrow tb)$	97.09	48.26
$\mathcal{BR}(H^+ \rightarrow \tau\nu)$	2.71	0.00
$\mathcal{BR}(H^+ \rightarrow W^+A)$	0.00	51.64
$\mathcal{BR}(B \rightarrow XY)$ in %		
$\mathcal{BR}(B \rightarrow W^+t)$	47.69	29.31
$\mathcal{BR}(B \rightarrow W^+T)$	-	-
$\mathcal{BR}(B \rightarrow Zb)$	21.26	14.09
$\mathcal{BR}(B \rightarrow hb)$	20.69	13.96
$\mathcal{BR}(B \rightarrow Hb)$	4.98	10.62
$\mathcal{BR}(B \rightarrow Ab)$	5.04	12.85
$\mathcal{BR}(B \rightarrow H^-t)$	0.30	19.14
$\mathcal{BR}(B \rightarrow H^-T)$	-	-
Γ in GeV		
$\Gamma(B)$	0.25	35.21

Table 6: The full description of our BPs for the (TBY) triplet case.

4 Conclusions

The third generation quarks of the SM, top and bottom, are often associated to SM extensions involving VLQs with the same EM charge, with which they can mix and thus interact, thereby mutually affecting their phenomenology. While this approach has been commonly exploited in the case of a SM-like Higgs sector, the relevance of these new states of Nature could actually be more important in the case of BSM scenarios with an extended Higgs sector, as VLQs and companion Higgs states can also interact with each other rather strongly. Furthermore, VLQs with exotic charges can belong to the same representation, thereby also entering the model phenomenology.

Specifically, in this paper, we have considered a 2HDM of Type-II supplemented by a VLB companion, alongside other new fermionic states (T , X and Y), of the SM falling in a singlet, doublet or triplet representation, in appropriate combinations. After constraining the parameter space of this model for all VLQ multiplet cases against the latest theoretical and experimental constraints, we have eventually proceeded to tension the ‘standard’ decays $B \rightarrow W^+t, Zb$ and hb (with h being the discovered SM-like Higgs state) against the ‘exotic’ ones $B \rightarrow H^+t, Ab$ and Hb (where H^+ , A and H are the heavy Higgs states of the 2HDM). Also notice that T states were not considered amongst the decay products of the B ones, because of the strong mass degeneracy between these (also involving, in part, the exotic VLQ states X and Y).

In doing so, we have come to the following broad conclusions.

- The simultaneous presence of a VLB and additional heavy Higgs boson loops as well as of their mixing effects with b and h states of the SM in the calculation of the EWPOs (i.e., the S, T and U parameters) has enabled us to access a much wider portion of parameter space than would otherwise been possible if only the separate effects of, on the one hand, B and, on the other hand, H^+ , A and H states had been considered. In particular, this opens up parameter space wherein B , as well as H^+ , A and H particles, can be light enough to be pursued in direct searches at the LHC, following $B\bar{B}$ pair production via QCD.
- The ability to access the aforementioned B exotic decays (and measure their relative rates) could allow one, in the presence of mass measurements of the Higgs states, to disentangle the underlying VLQ multiplet structure, whether singlet, doublet or triplet, thereby greatly characterizing the underlying BSM scenario, including confirming its Type-II nature and measure the key parameters of our 2HDM+VLQ model.

We have come to these conclusions by performing an inclusive analysis at the cross-section and \mathcal{BR} level, without any MC simulations. We advocate the latter as the next step to carry out a vigorous research programme testing the possibility of both an extended Higgs sector and an enlarged fermionic spectrum being simultaneously accessible at the LHC through non-SM like signatures of a VLB produced in pairs in QCD collisions. To this end, we have proposed several BPs amenable to experimental investigation during Run 3 of the LHC and/or its high luminosity phase.

Acknowledgments

The work of AB, RB and MB is supported by the Moroccan Ministry of Higher Education and Scientific Research MESRSFC and CNRST Project PPR/2015/6. SM is supported in part through the NExT Institute, STFC Consolidated Grant ST/L000296/1 and Knut and Alice Wallenberg foundation under the grant KAW 2017.0100 (SHIFT).

Appendix

4.1 Lagrangian in the mass basis

After EWSB, we are left with five Higgs bosons that are two-CP even h and H , one CP-odd A , and then a pair of charged Higgs H^\pm . We now collect the Lagrangian on the mass basis in the general 2HDM Type-II.

4.2 Light-light interactions

$$\begin{aligned}
\mathcal{L}_W &= -\frac{g}{\sqrt{2}}\bar{t}\gamma^\mu(V_{tb}^L P_L + V_{tb}^R P_R)bW_\mu^+ + H.c., \\
\mathcal{L}_Z &= -\frac{g}{2c_W}\bar{t}\gamma^\mu(X_{tt}^L P_L + X_{tt}^R P_R - 2Q_t s_W^2)tZ_\mu \\
&\quad -\frac{g}{2c_W}\bar{b}\gamma^\mu(-X_{bb}^L P_L - X_{bb}^R P_R - 2Q_b s_W^2)bZ_\mu + H.c., \\
\mathcal{L}_{h^0} &= -\frac{gm_t}{2M_W}Y_{tt}^h\bar{t}t h^0 - \frac{gm_b}{2M_W}Y_{bb}^h\bar{b}b h^0 + H.c., \\
\mathcal{L}_{H^0} &= -\frac{gm_t}{2M_W}Y_{tt}^H\bar{t}t H^0 - \frac{gm_b}{2M_W}Y_{bb}^H\bar{b}b H^0 + H.c., \\
\mathcal{L}_A &= -i\frac{gm_t}{2M_W}Y_{tt}^A\bar{t}\gamma_5 t A + i\frac{gm_b}{2M_W}Y_{bb}^A\bar{b}\gamma_5 b A + H.c., \\
\mathcal{L}_{H^\pm} &= -\frac{gm_t}{\sqrt{2}M_W}\bar{t}(\cot\beta Z_{tb}^L P_L + \tan\beta Z_{tb}^R P_R)bH^\pm + H.c.
\end{aligned} \tag{22}$$

	V_{tb}^L	V_{tb}^R
(B)	c_L	0
(TB)	$c_L^u c_L^d + s_L^u s_L^d e^{i(\phi_u - \phi_d)}$	$s_R^u s_R^d e^{i(\phi_u - \phi_d)}$
(BY)	c_L	0
(XTB)	$c_L^u c_L^d + \sqrt{2}s_L^u s_L^d$	$\sqrt{2}s_R^u s_R^d$
(TBY)	$c_L^u c_L^d + \sqrt{2}s_L^u s_L^d$	$\sqrt{2}s_R^u s_R^d$

Table VII: Light-light couplings to the W boson.

	X_{tt}^L	X_{tt}^R	X_{bb}^L	X_{bb}^R
(B)	1	0	c_L^2	0
(TB)	1	$(s_R^u)^2$	1	$(s_R^d)^2$
(BY)	1	0	$c_L^2 - s_L^2$	$-s_R^2$
(XTB)	$(c_L^u)^2$	0	$1 + (s_L^d)^2$	$2(s_R^d)^2$
(TBY)	$1 + (s_L^u)^2$	$2(s_R^u)^2$	$(c_L^d)^2$	0

Table VIII: Light-light couplings to the Z boson.

	Y_{tt}^h	Y_{tt}^H	Y_{tt}^A
(B)	$s_{\beta\alpha} + c_{\beta\alpha} \cot \beta$	$c_{\beta\alpha} - s_{\beta\alpha} \cot \beta$	$-\cot \beta$
(TB)	$(s_{\beta\alpha} + c_{\beta\alpha} \cot \beta)(c_R^u)^2$	$(c_{\beta\alpha} - s_{\beta\alpha} \cot \beta)(c_R^u)^2$	$-\cot \beta (c_R^u)^2$
(BY)	$s_{\beta\alpha} + c_{\beta\alpha} \cot \beta$	$c_{\beta\alpha} - s_{\beta\alpha} \cot \beta$	$-\cot \beta$
(XTB)	$(s_{\beta\alpha} + c_{\beta\alpha} \cot \beta)(c_L^u)^2$	$(c_{\beta\alpha} - s_{\beta\alpha} \cot \beta)(c_L^u)^2$	$-\cot \beta (c_L^u)^2$
(TBY)	$(s_{\beta\alpha} + c_{\beta\alpha} \cot \beta)(c_L^u)^2$	$(c_{\beta\alpha} - s_{\beta\alpha} \cot \beta)(c_L^u)^2$	$-\cot \beta (c_L^u)^2$

 Table IX: Light-light top quark couplings to the triplets Higgs $\{h, H, A\}$.

	Y_{bb}^h	Y_{bb}^H	Y_{bb}^A
(B)	$(s_{\beta\alpha} - c_{\beta\alpha} \tan \beta)c_L^2$	$(c_{\beta\alpha} + s_{\beta\alpha} \tan \beta)c_L^2$	$\tan \beta c_L^2$
(TB)	$(s_{\beta\alpha} - c_{\beta\alpha} \tan \beta)(c_R^d)^2$	$(c_{\beta\alpha} + s_{\beta\alpha} \tan \beta)(c_R^d)^2$	$\tan \beta (c_R^d)^2$
(BY)	$(s_{\beta\alpha} - c_{\beta\alpha} \tan \beta)c_R^2$	$(c_{\beta\alpha} + s_{\beta\alpha} \tan \beta)c_R^2$	$\tan \beta c_R^2$
(XTB)	$(s_{\beta\alpha} - c_{\beta\alpha} \tan \beta)(c_L^d)^2$	$(c_{\beta\alpha} + s_{\beta\alpha} \tan \beta)(c_L^d)^2$	$\tan \beta (c_L^d)^2$
(TBY)	$(s_{\beta\alpha} - c_{\beta\alpha} \tan \beta)(c_L^d)^2$	$(c_{\beta\alpha} + s_{\beta\alpha} \tan \beta)(c_L^d)^2$	$\tan \beta (c_L^d)^2$

 Table X: Light-light bottom quark couplings to the triplets Higgs $\{h, H, A\}$.

	Z_{tb}^L	Z_{tb}^R
(B)	c_L	$\frac{m_t}{m_B} c_L$
(TB)	$c_L^d c_L^u + \frac{s_L^d}{s_L^u} (s_L^{u2} - s_R^{u2}) e^{i(\phi_u - \phi_d)}$	$\frac{m_b}{m_t} \left[c_L^u c_L^d + \frac{s_L^u}{s_L^d} (s_L^{d2} - s_R^{d2}) e^{i(\phi_u - \phi_d)} \right]$
(BY)	c_R	c_L
(XTB)	c_L^u	c_L^d
(TBY)	c_L^u	c_L^d

Table XI: Light-light couplings to the charged Higgs.

4.3 Heavy-heavy interactions

$$\begin{aligned}
 \mathcal{L}_W &= -\frac{g}{\sqrt{2}} \bar{Q} \gamma^\mu (V_{QQ'}^L P_L + V_{QQ'}^R P_R) Q' W_\mu^+ + H.c., \\
 \mathcal{L}_Z &= -\frac{g}{2c_W} \bar{Q} \gamma^\mu (\pm X_{QQ}^L P_L \pm X_{QQ}^R P_R - 2Q_Q s_W^2) Q Z_\mu \\
 \mathcal{L}_{h^0} &= -\frac{gm_Q}{2M_W} Y_{QQ}^h \bar{Q} Q h^0 + H.c., \\
 \mathcal{L}_{H^0} &= -\frac{gm_Q}{2M_W} Y_{QQ}^H \bar{Q} Q H^0 + H.c., \\
 \mathcal{L}_A &= \pm i \frac{gm_Q}{2M_W} Y_{QQ}^A \bar{Q} \gamma_5 Q A + H.c., \\
 \mathcal{L}_{H^\pm} &= -\frac{gm_Q}{\sqrt{2}M_W} \bar{Q} (\cot \beta Z_{QQ}^L P_L + \tan \beta Z_{QQ}^R P_R) Q H^\pm + H.c.
 \end{aligned} \tag{23}$$

	V_{TB}^L	V_{TB}^R	V_{BY}^L	V_{BY}^R
(TB)	$s_L^u s_L^d e^{-i(\phi_u - \phi_d)} + c_L^u c_L^d$	$c_R^u c_R^d$	—	—
(BY)	—	—	c_L	c_R
(XTB)	$s_L^u s_L^d + \sqrt{2} c_L^u c_L^d$	$\sqrt{2} c_R^u c_R^d$	—	—
(TBY)	$s_L^u s_L^d + \sqrt{2} c_L^u c_L^d$	$\sqrt{2} c_R^u c_R^d$	$\sqrt{2} c_L^d$	$\sqrt{2} c_R^d$

Table XII: Heavy-heavy couplings to the W boson.

	X_{BB}^L	X_{BB}^R
(B)	$(s_L)^2$	0
(TB)	1	$(c_R^d)^2$
(BY)	$s_L^2 - c_L^2$	$-c_R^2$
(XTB)	$1 + (c_L^d)^2$	$2(c_R^d)^2$
(TBY)	$(s_L^d)^2$	0

 Table XIII: Heavy-heavy couplings to the Z boson.

	Y_{BB}^h	Y_{BB}^H	Y_{BB}^A	$Y_{YY}^{\{h,H,A\}}$
(B)	$(s_{\beta\alpha} - c_{\beta\alpha} \tan \beta) s_L^2$	$(c_{\beta\alpha} + s_{\beta\alpha} \tan \beta) s_L^2$	$\tan \beta s_L^2$	—
(TB)	$(s_{\beta\alpha} - c_{\beta\alpha} \tan \beta) (s_R^d)^2$	$(c_{\beta\alpha} + s_{\beta\alpha} \tan \beta) (s_R^d)^2$	$\tan \beta (s_R^d)^2$	—
(BY)	$(s_{\beta\alpha} - c_{\beta\alpha} \tan \beta) s_R^2$	$(c_{\beta\alpha} + s_{\beta\alpha} \tan \beta) s_R^2$	$\tan \beta s_R^2$	0
(XTB)	$(s_{\beta\alpha} - c_{\beta\alpha} \tan \beta) (s_L^d)^2$	$(c_{\beta\alpha} + s_{\beta\alpha} \tan \beta) (s_L^d)^2$	$\tan \beta (s_L^d)^2$	—
(TBY)	$(s_{\beta\alpha} - c_{\beta\alpha} \tan \beta) (s_L^d)^2$	$(c_{\beta\alpha} + s_{\beta\alpha} \tan \beta) (s_L^d)^2$	$\tan \beta (s_L^d)^2$	0

 Table XIV: Heavy-heavy Bottom VLQ couplings to the triplets Higgs $\{h, H, A\}$.

	Z_{TB}^L	Z_{TB}^R	Z_{BY}^L	Z_{BY}^R
(TB)	$s_L^d s_L^u e^{i(\phi_d - \phi_u)} + \frac{c_L^d}{c_L^u} (s_R^{u2} - s_L^{u2})$	$\frac{m_B}{m_T} \left[s_L^u s_L^d e^{i(\phi_d - \phi_u)} + \frac{c_L^u}{c_L^d} (s_R^{d2} - s_L^{d2}) \right]$	—	—
(XTB)	—	—	—	—
(TBY)	—	—	$s_L e^{-i\phi}$	0

Table XV: Heavy-heavy couplings to the charged Higgs.

4.4 Light-heavy interactions

$$\begin{aligned}
 \mathcal{L}_W &= -\frac{g}{\sqrt{2}} \bar{Q} \gamma^\mu (V_{Qq}^L P_L + V_{Qq}^R P_R) q W_\mu^+ \\
 &\quad -\frac{g}{\sqrt{2}} \bar{q} \gamma^\mu (V_{qQ}^L P_L + V_{qQ}^R P_R) Q W_\mu^+ + H.c. \\
 \mathcal{L}_Z &= -\frac{g}{2c_W} \bar{q} \gamma^\mu (\pm X_{qQ}^L P_L \pm X_{qQ}^R P_R) Q Z_\mu + H.c. \\
 \mathcal{L}_{h^0} &= -\frac{gm_T}{2M_W} \bar{t} (Y_{htT}^L P_L + Y_{htT}^R P_R) T h^0 \\
 &\quad -\frac{gm_B}{2M_W} \bar{b} (Y_{hbB}^L P_L + Y_{hbB}^R P_R) B h^0 + H.c. \\
 \mathcal{L}_{H^0} &= -\frac{gm_T}{2M_W} \bar{t} (Y_{HtT}^L P_L + Y_{HtT}^R P_R) T H^0 \\
 &\quad -\frac{gm_B}{2M_W} \bar{b} (Y_{HbB}^L P_L + Y_{HbB}^R P_R) B H^0 + H.c. \\
 \mathcal{L}_A &= i \frac{gm_T}{2M_W} \bar{t} (Y_{AtT}^L P_L - Y_{AtT}^R P_R) T A \\
 &\quad -i \frac{gm_B}{2M_W} \bar{b} (Y_{AbB}^L P_L - Y_{AbB}^R P_R) B A + H.c. \\
 \mathcal{L}_{H^\pm} &= -\frac{gm_T}{\sqrt{2}M_W} \bar{T} (\cot \beta Z_{Tb}^L P_L + \tan \beta Z_{Tb}^R P_R) b H^\pm
 \end{aligned}$$

$$-\frac{gm_B}{\sqrt{2}M_W}\bar{t}(\cot\beta Z_{tB}^L P_L + \tan\beta Z_{tB}^R P_R)BH^+ + H.c. \quad (24)$$

	V_{tB}^L	V_{tB}^R	V_{bY}^L	V_{bY}^R
(B)	$s_L e^{i\phi}$	0	—	—
(TB)	$c_L^u s_L^d e^{i\phi_d} - s_L^u c_L^d e^{i\phi_u}$	$-s_R^u c_R^d e^{i\phi_u}$	—	—
(BY)	$s_L e^{i\phi}$	0	$-s_L e^{i\phi}$	$-s_R e^{i\phi}$
(XTB)	$(c_L^u s_L^d - \sqrt{2}s_L^u c_L^d)e^{i\phi}$	$-\sqrt{2}s_R^u c_R^d e^{i\phi}$	—	—
(TBY)	$(c_L^u s_L^d - \sqrt{2}s_L^u c_L^d)e^{i\phi}$	$-\sqrt{2}s_R^u c_R^d e^{i\phi}$	$-\sqrt{2}s_L^d e^{i\phi}$	$-\sqrt{2}s_R^d e^{i\phi}$

Table XVI: Light-heavy couplings to the W boson.

	X_{bB}^L	X_{bB}^R
(B)	$c_L s_L e^{i\phi}$	0
(TB)	0	$-s_R^d c_R^d e^{i\phi_d}$
(BY)	$2c_L s_L e^{i\phi}$	$c_R s_R e^{i\phi}$
(XTB)	$-s_L^d c_L^d e^{i\phi}$	$-2s_R^d c_R^d e^{i\phi}$
(TBY)	$s_L^d c_L^d e^{i\phi}$	0

Table XVII: Light-heavy couplings to the Z boson.

	Y_{hbB}^L	Y_{HbB}^L	Y_{AbB}^L
(B)	$(s_{\beta\alpha} - c_{\beta\alpha} \tan\beta) \frac{m_b}{m_B} c_L s_L e^{i\phi}$	$(c_{\beta\alpha} + s_{\beta\alpha} \tan\beta) \frac{m_b}{m_B} c_L s_L e^{i\phi}$	$\tan\beta \frac{m_b}{m_B} c_L s_L e^{i\phi}$
(TB)	$(s_{\beta\alpha} - c_{\beta\alpha} \tan\beta) s_R^d c_R^d e^{i\phi_d}$	$(c_{\beta\alpha} + s_{\beta\alpha} \tan\beta) s_R^d c_R^d e^{i\phi_d}$	$\tan\beta s_R^d c_R^d e^{i\phi_d}$
(BY)	$(s_{\beta\alpha} - c_{\beta\alpha} \tan\beta) c_R s_R e^{i\phi}$	$(c_{\beta\alpha} + s_{\beta\alpha} \tan\beta) c_R s_R e^{i\phi}$	$\tan\beta c_R s_R e^{i\phi}$
(XTB)	$(s_{\beta\alpha} - c_{\beta\alpha} \tan\beta) \frac{m_b}{m_B} s_L^d c_L^d e^{i\phi}$	$(c_{\beta\alpha} + s_{\beta\alpha} \tan\beta) \frac{m_b}{m_B} s_L^d c_L^d e^{i\phi}$	$\tan\beta \frac{m_b}{m_B} s_L^d c_L^d e^{i\phi}$
(TBY)	$(s_{\beta\alpha} - c_{\beta\alpha} \tan\beta) \frac{m_b}{m_B} s_L^d c_L^d e^{i\phi}$	$(c_{\beta\alpha} + s_{\beta\alpha} \tan\beta) \frac{m_b}{m_B} s_L^d c_L^d e^{i\phi}$	$\tan\beta \frac{m_b}{m_B} s_L^d c_L^d e^{i\phi}$

Table XVIII: Light-heavy left couplings of Bottom quarks to the triplets Higgs $\{h, H, A\}$.

	Y_{hbB}^R	Y_{HbB}^R	Y_{AbB}^R
(B)	$(s_{\beta\alpha} - c_{\beta\alpha} \tan\beta) c_L s_L e^{i\phi}$	$(c_{\beta\alpha} + s_{\beta\alpha} \tan\beta) c_L s_L e^{i\phi}$	$\tan\beta c_L s_L e^{i\phi}$
(TB)	$(s_{\beta\alpha} - c_{\beta\alpha} \tan\beta) \frac{m_b}{m_B} s_R^d c_R^d e^{i\phi_d}$	$(c_{\beta\alpha} + s_{\beta\alpha} \tan\beta) \frac{m_b}{m_B} s_R^d c_R^d e^{i\phi_d}$	$\tan\beta \frac{m_b}{m_B} s_R^d c_R^d e^{i\phi_d}$
(BY)	$(s_{\beta\alpha} - c_{\beta\alpha} \tan\beta) \frac{m_b}{m_B} c_R s_R e^{i\phi}$	$(c_{\beta\alpha} + s_{\beta\alpha} \tan\beta) \frac{m_b}{m_B} c_R s_R e^{i\phi}$	$\tan\beta \frac{m_b}{m_B} c_R s_R e^{i\phi}$
(XTB)	$(s_{\beta\alpha} - c_{\beta\alpha} \tan\beta) s_L^d c_L^d e^{i\phi}$	$(c_{\beta\alpha} + s_{\beta\alpha} \tan\beta) s_L^d c_L^d e^{i\phi}$	$\tan\beta s_L^d c_L^d e^{i\phi}$
(TBY)	$(s_{\beta\alpha} - c_{\beta\alpha} \tan\beta) s_L^d c_L^d e^{i\phi}$	$(c_{\beta\alpha} + s_{\beta\alpha} \tan\beta) s_L^d c_L^d e^{i\phi}$	$\tan\beta s_L^d c_L^d e^{i\phi}$

Table XIX: Light-heavy right couplings of Bottom quarks to the triplets Higgs $\{h, H, A\}$.

	Z_{bY}^L	Z_{bY}^R	Z_{tB}^L	Z_{tB}^R
(B)	—	—	s_L	0
(BY)	$s_R e^{-i\phi}$	0	0	0
(TB)	—	—	$\frac{m_t}{m_B} \left[c_L^u s_L^d e^{i\phi_d} + (s_R^{u2} - s_L^{u2}) \frac{c_L^d}{s_L^u} e^{i\phi_u} \right]$	$c_L^u s_L^d e^{i\phi_d} + (s_L^{d2} - s_R^{d2}) \frac{s_L^u}{c_L^d} e^{i\phi_u}$
(TBY)	c_L^u	0	s_L^d	0

Table XX: Light-heavy couplings to the charged Higgs.

References

- [1] **ATLAS** collaboration, *Observation of a new particle in the search for the Standard Model Higgs boson with the ATLAS detector at the LHC*, *Phys. Lett. B* **716** (2012) 1 [[1207.7214](#)].
- [2] **CMS** collaboration, *Observation of a New Boson at a Mass of 125 GeV with the CMS Experiment at the LHC*, *Phys. Lett. B* **716** (2012) 30 [[1207.7235](#)].
- [3] A. Arhrib, R. Benbrik, M. Boukidi, B. Manaut and S. Moretti, *Anatomy of Vector-Like Top-Quark Models in the Alignment Limit of the 2-Higgs Doublet Model Type-II*, [2401.16219](#).
- [4] G.C. Branco, P.M. Ferreira, L. Lavoura, M.N. Rebelo, M. Sher and J.P. Silva, *Theory and phenomenology of two-Higgs-doublet models*, *Phys. Rept.* **516** (2012) 1 [[1106.0034](#)].
- [5] P. Draper, A. Ekstedt and H.E. Haber, *A natural mechanism for approximate Higgs alignment in the 2HDM*, *JHEP* **05** (2021) 235 [[2011.13159](#)].
- [6] R. Benbrik, C.-H. Chen and T. Nomura, *Higgs singlet boson as a diphoton resonance in a vectorlike quark model*, *Phys. Rev. D* **93** (2016) 055034 [[1512.06028](#)].
- [7] A. Arhrib, R. Benbrik, S.J.D. King, B. Manaut, S. Moretti and C.S. Un, *Phenomenology of 2HDM with vectorlike quarks*, *Phys. Rev. D* **97** (2018) 095015 [[1607.08517](#)].
- [8] J.A. Aguilar-Saavedra, R. Benbrik, S. Heinemeyer and M. Pérez-Victoria, *Handbook of vectorlike quarks: Mixing and single production*, *Phys. Rev. D* **88** (2013) 094010 [[1306.0572](#)].
- [9] M. Badziak, *Interpreting the 750 GeV diphoton excess in minimal extensions of Two-Higgs-Doublet models*, *Phys. Lett. B* **759** (2016) 464 [[1512.07497](#)].
- [10] A. Angelescu, A. Djouadi and G. Moreau, *Scenarii for interpretations of the LHC diphoton excess: two Higgs doublets and vector-like quarks and leptons*, *Phys. Lett. B* **756** (2016) 126 [[1512.04921](#)].
- [11] J.A. Aguilar-Saavedra, *Identifying top partners at LHC*, *JHEP* **11** (2009) 030 [[0907.3155](#)].
- [12] A. De Simone, O. Matsedonskyi, R. Rattazzi and A. Wulzer, *A First Top Partner Hunter's Guide*, *JHEP* **04** (2013) 004 [[1211.5663](#)].
- [13] S. Kanemura, M. Kikuchi and K. Yagyu, *Fingerprinting the extended Higgs sector using one-loop corrected Higgs boson couplings and future precision measurements*, *Nucl. Phys. B* **896** (2015) 80 [[1502.07716](#)].
- [14] L. Lavoura and J.P. Silva, *The Oblique corrections from vector - like singlet and doublet quarks*, *Phys. Rev. D* **47** (1993) 2046.
- [15] C.-Y. Chen, S. Dawson and E. Furlan, *Vectorlike fermions and Higgs effective field theory revisited*, *Phys. Rev. D* **96** (2017) 015006 [[1703.06134](#)].
- [16] A. Carvalho, S. Moretti, D. O'Brien, L. Panizzi and H. Prager, *Single production of vectorlike quarks with large width at the Large Hadron Collider*, *Phys. Rev. D* **98** (2018) 015029 [[1805.06402](#)].
- [17] S. Moretti, D. O'Brien, L. Panizzi and H. Prager, *Production of extra quarks at the Large Hadron Collider beyond the Narrow Width Approximation*, *Phys. Rev. D* **96** (2017) 075035 [[1603.09237](#)].
- [18] H. Prager, S. Moretti, D. O'Brien and L. Panizzi, *Large width effects in processes of production of extra quarks decaying to Dark Matter at the LHC*, *PoS DIS2017* (2018) 300 [[1706.04007](#)].

- [19] H. Prager, S. Moretti, D. O'Brien and L. Panizzi, *Extra Quarks Decaying to Dark Matter Beyond the Narrow Width Approximation*, in *5th Large Hadron Collider Physics Conference*, 6, 2017 [[1706.04001](#)].
- [20] S. Moretti, D. O'Brien, L. Panizzi and H. Prager, *Production of extra quarks decaying to Dark Matter beyond the Narrow Width Approximation at the LHC*, *Phys. Rev. D* **96** (2017) 035033 [[1705.07675](#)].
- [21] A. Deandrea and A.M. Iyer, *Vectorlike quarks and heavy colored bosons at the LHC*, *Phys. Rev. D* **97** (2018) 055002 [[1710.01515](#)].
- [22] J.A. Aguilar-Saavedra, D.E. López-Fogliani and C. Muñoz, *Novel signatures for vector-like quarks*, *JHEP* **06** (2017) 095 [[1705.02526](#)].
- [23] J.a.M. Alves, G.C. Branco, A.L. Cherchiglia, C.C. Nishi, J.T. Penedo, P.M.F. Pereira et al., *Vector-like singlet quarks: A roadmap*, *Phys. Rept.* **1057** (2024) 1 [[2304.10561](#)].
- [24] R. Dermíšek, E. Lunghi and S. Shin, *Hunting for Vectorlike Quarks*, *JHEP* **04** (2019) 019 [[1901.03709](#)].
- [25] R. Dermisek, E. Lunghi, N. McGinnis and S. Shin, *Signals with six bottom quarks for charged and neutral Higgs bosons*, *JHEP* **07** (2020) 241 [[2005.07222](#)].
- [26] R. Dermisek, E. Lunghi, N. McGinnis and S. Shin, *Tau-jet signatures of vectorlike quark decays to heavy charged and neutral Higgs bosons*, *JHEP* **08** (2021) 159 [[2105.10790](#)].
- [27] R. Benbrik, M. Boukidi and S. Moretti, *Probing Light Charged Higgs Bosons in the 2-Higgs Doublet Model Type-II with Vector-Like Quarks*, [2211.07259](#).
- [28] D. Eriksson, J. Rathsman and O. Stal, *2HDMC: Two-Higgs-Doublet Model Calculator Physics and Manual*, *Comput. Phys. Commun.* **181** (2010) 189 [[0902.0851](#)].
- [29] C. Degrande, C. Duhr, B. Fuks, D. Grellscheid, O. Mattelaer and T. Reiter, *UFO - The Universal FeynRules Output*, *Comput. Phys. Commun.* **183** (2012) 1201 [[1108.2040](#)].
- [30] T. Hahn, *Generating Feynman diagrams and amplitudes with FeynArts 3*, *Comput. Phys. Commun.* **140** (2001) 418 [[hep-ph/0012260](#)].
- [31] J. Kublbeck, M. Bohm and A. Denner, *Feyn Arts: Computer Algebraic Generation of Feynman Graphs and Amplitudes*, *Comput. Phys. Commun.* **60** (1990) 165.
- [32] T. Hahn and C. Schappacher, *The Implementation of the minimal supersymmetric standard model in FeynArts and FormCalc*, *Comput. Phys. Commun.* **143** (2002) 54 [[hep-ph/0105349](#)].
- [33] T. Hahn and M. Perez-Victoria, *Automatized one loop calculations in four-dimensions and D-dimensions*, *Comput. Phys. Commun.* **118** (1999) 153 [[hep-ph/9807565](#)].
- [34] J. Alwall, R. Frederix, S. Frixione, V. Hirschi, F. Maltoni, O. Mattelaer et al., *The automated computation of tree-level and next-to-leading order differential cross sections, and their matching to parton shower simulations*, *JHEP* **07** (2014) 079 [[1405.0301](#)].
- [35] H. Abouabid, A. Arhrib, R. Benbrik, M. Boukidi and J.E. Falaki, *The oblique parameters in the 2HDM with Vector-Like Quarks: Confronting M_W CDF-II Anomaly*, [2302.07149](#).
- [36] S.-P. He, *Leptoquark and vector-like quark extended model for simultaneous explanation of W boson mass and muon $g-2$ anomalies**, *Chin. Phys. C* **47** (2023) 043102 [[2205.02088](#)].
- [37] J. Cao, L. Meng, L. Shang, S. Wang and B. Yang, *Interpreting the W -mass anomaly in vectorlike quark models*, *Phys. Rev. D* **106** (2022) 055042 [[2204.09477](#)].

- [38] S. Kanemura, T. Kubota and E. Takasugi, *Lee-Quigg-Thacker bounds for Higgs boson masses in a two doublet model*, *Phys. Lett. B* **313** (1993) 155 [[hep-ph/9303263](#)].
- [39] A. Barroso, P.M. Ferreira, I.P. Ivanov and R. Santos, *Metastability bounds on the two Higgs doublet model*, *JHEP* **06** (2013) 045 [[1303.5098](#)].
- [40] N.G. Deshpande and E. Ma, *Pattern of Symmetry Breaking with Two Higgs Doublets*, *Phys. Rev. D* **18** (1978) 2574.
- [41] W. Grimus, L. Lavoura, O.M. Ogreid and P. Osland, *A Precision constraint on multi-Higgs-doublet models*, *J. Phys. G* **35** (2008) 075001 [[0711.4022](#)].
- [42] M.J. Molewski and B.J.P. Jones, *Scalable qubit representations of neutrino mixing matrices*, *Phys. Rev. D* **105** (2022) 056024 [[2111.05401](#)].
- [43] P. Bechtle, D. Dercks, S. Heinemeyer, T. Klingl, T. Stefaniak, G. Weiglein et al., *HiggsBounds-5: Testing Higgs Sectors in the LHC 13 TeV Era*, *Eur. Phys. J. C* **80** (2020) 1211 [[2006.06007](#)].
- [44] P. Bechtle, S. Heinemeyer, T. Klingl, T. Stefaniak, G. Weiglein and J. Wittbrodt, *HiggsSignals-2: Probing new physics with precision Higgs measurements in the LHC 13 TeV era*, *Eur. Phys. J. C* **81** (2021) 145 [[2012.09197](#)].
- [45] H. Bahl, T. Biekötter, S. Heinemeyer, C. Li, S. Paasch, G. Weiglein et al., *HiggsTools: BSM scalar phenomenology with new versions of HiggsBounds and HiggsSignals*, *Comput. Phys. Commun.* **291** (2023) 108803 [[2210.09332](#)].
- [46] P. Bechtle, O. Brein, S. Heinemeyer, G. Weiglein and K.E. Williams, *HiggsBounds: Confronting Arbitrary Higgs Sectors with Exclusion Bounds from LEP and the Tevatron*, *Comput. Phys. Commun.* **181** (2010) 138 [[0811.4169](#)].
- [47] P. Bechtle, O. Brein, S. Heinemeyer, G. Weiglein and K.E. Williams, *HiggsBounds 2.0.0: Confronting Neutral and Charged Higgs Sector Predictions with Exclusion Bounds from LEP and the Tevatron*, *Comput. Phys. Commun.* **182** (2011) 2605 [[1102.1898](#)].
- [48] P. Bechtle, O. Brein, S. Heinemeyer, O. Stål, T. Stefaniak, G. Weiglein et al., *HiggsBounds – 4: Improved Tests of Extended Higgs Sectors against Exclusion Bounds from LEP, the Tevatron and the LHC*, *Eur. Phys. J. C* **74** (2014) 2693 [[1311.0055](#)].
- [49] P. Bechtle, S. Heinemeyer, O. Stal, T. Stefaniak and G. Weiglein, *Applying Exclusion Likelihoods from LHC Searches to Extended Higgs Sectors*, *Eur. Phys. J. C* **75** (2015) 421 [[1507.06706](#)].
- [50] A. Djouadi, *The Anatomy of electro-weak symmetry breaking. I: The Higgs boson in the standard model*, *Phys. Rept.* **457** (2008) 1 [[hep-ph/0503172](#)].
- [51] J. Pumplin, D.R. Stump, J. Huston, H.L. Lai, P.M. Nadolsky and W.K. Tung, *New generation of parton distributions with uncertainties from global QCD analysis*, *JHEP* **07** (2002) 012 [[hep-ph/0201195](#)].
- [52] M. Czakon and A. Mitov, *Top++: A Program for the Calculation of the Top-Pair Cross-Section at Hadron Colliders*, *Comput. Phys. Commun.* **185** (2014) 2930 [[1112.5675](#)].
- [53] **ATLAS** collaboration, *Search for charged Higgs bosons decaying into a top-quark and a bottom-quark at $\sqrt{s} = 13$ TeV with the ATLAS detector*, .
- [54] **ATLAS** collaboration, *Search for heavy Higgs bosons decaying into two tau leptons with the ATLAS detector using pp collisions at $\sqrt{s} = 13$ TeV*, *Phys. Rev. Lett.* **125** (2020) 051801 [[2002.12223](#)].